Chapter 3
Chemical Reduction and Oxidation of Organic Contaminants by Nanoscale Zerovalent Iron

Tanapon Phenrat, Thi Song Thao Le, Bhanuphong Naknakorn, and Gregory V. Lowry

Abstract This chapter critically reviews the kinetics of NZVI used to reductively and oxidatively transform various kinds of priority organic contaminants including chlorinated ethenes, chlorinated ethanes, chlorinated and aromatic nitro hydrocarbons, chlorinated biphenyls, halogenated bisphenol A, explosives, dyes, and pesticides. All kinds of NZVI, including bare, bimetallic, polymer-modified, and supported NZVI, are reviewed. A total of 102 datasets of laboratory-scale experiments over 20 years (1997–2017) of NZVI research are evaluated to extract state-of-the-art understanding. This chapter elaborates not only reductive transformation pathways of priority organic contaminants but also two factors governing NZVI reactivity: intrinsic properties of the materials and environmental conditions where NZVI particles are applied. These include the particle crystallinity and chemical composition (noble metal), the effect of polymeric surface modification, and the effects of sorptive support, aging effects, pH, anionic and cationic solutes, natural organic matter, aquifer material, contaminant concentration, and the presence of

T. Phenrat (✉) · T. S. T. Le
Department of Civil Engineering, Environmental Engineering Program, Naresuan University, Phitsanulok, Thailand

Center of Excellence for Sustainability of Health, Environment and Industry (SHEI), Faculty of Engineering, Naresuan University, Phitsanulok, Thailand

B. Naknakorn
Thai Plastic and Chemicals PCL, Bangkok, Thailand

Center for Environmental Implications of Nanotechnology (CEINT)
Carnegie Mellon University, Pittsburgh, PA, USA

G. V. Lowry
Center for Environmental Implications of Nanotechnology (CEINT)
Carnegie Mellon University, Pittsburgh, PA, USA

Department of Civil & Environmental Engineering, Carnegie Mellon University, Pittsburgh, PA, USA

T. Phenrat, G. V. Lowry (eds.), *Nanoscale Zerovalent Iron Particles for Environmental Restoration*, https://doi.org/10.1007/978-3-319-95340-3_3

dense nonaqueous phase liquid. Similarly, various factors affecting oxidative degradation of contaminants of concern using NZVI-induced Fenton's reaction are reviewed.

Keywords Nanoscale zerovalent iron · Reductive dechlorination · Fenton reaction · Chlorinated organics · Degradation kinetics · Degradation mechanisms

3.1 Reductive Transformation of Priority Organic Contaminants Using Nanoscale Zerovalent Iron

Nanoscale zerovalent iron (NZVI) is a well-known remediation agent due to its high reactivity to reductively detoxify a variety of contaminants, including metals (Chap. 4) and halogenated organics, which is the focus of this chapter. Table 3.1 provides an intensive review of the reductive transformation of priority organic contaminants, including chlorinated ethene, chlorinated ethane, chlorinated and aromatic nitro hydrocarbon, chlorinated biphenyl, halogenated bisphenol A, explosives, dye, and pesticides, using various kinds of NZVI, including bare, bimetallic, polymer-modified, and supported NZVI. This involves 102 datasets of laboratory-scaled experiments over 20 years (1997–2017) of NZVI research. In addition to presenting a database of organic contaminants, several interesting trends can be determined from Table 3.1, some of which will be discussed later in this chapter.

Although the idea of using NZVI for in situ subsurface remediation started in 1997 (Wang and Zhang 1997), bulk ZVI has long been recognized as an electron donor and has been used in the form of iron filings to build a permeable reactive barrier since 1994 (Reynolds et al. 1990; Gillham and O'Hannesin 1994). Undeniably, NZVI is much more reactive than its ZVI counterpart on the mass basis comparison. Nevertheless, it is still debatable if this is mainly due to a much larger specific surface area of NZVI in comparison to iron filings or micron-sized ZVI or if it has something to do with the "nano-effect," which may result in a greater density of reactive surface sites or surface sites of higher intrinsic reactivity.

The small size of nanoparticles causes an exponential increase in the number of atoms localized at the surface. These atoms are characterized by excess surface energy and are thermodynamically unstable (Ghosh 2015). This results in crystallographic changes including lattice contraction or deformation, the appearance of defects, rearrangements of the surface atoms, or changes in the morphology of nanoparticles (Jiang et al. 2001). This may yield quantum size effects, which cause changes in the Fermi level and band gap, leading to increases in intrinsic reactivity with decreasing particle size (Ghosh 2015).

Nevertheless, Tratnyek's group revealed that, for tetrachloromethane (or carbon tetrachloride (CT)), no "nano-effect" contributing to the greater intrinsic reactivity of the surface sites or the greater abundance of reactive sites on the surface was observed. This is because, when comparing surface-area normalized rate constants (k_{SA}) against mass normalized rate constants (k_M) for the reductive degradation of

Table 3.1 Summary of batch experiments for reductive treatment of organic contaminants using various NZVI (1997–2017)

No.	Contaminant (initial concentration)	Type of particle	Dispersant or supported material	Experimental condition	Rate constant (pseudo-first order)	Contaminant removal (%)	References
Chlorinated ethene							
1	Trichloroethylene (TCE) (7 mg/L)	Fe^{BH}	–	Batch experiment using 10 g/L bare and PV3A stabilized NZVI in deionized (DI) water	$k_{obs} = 4.11$/h per 10 g/L of NZVI	98% removal after 3 h	Sun et al. (2007)
2	TCE (7 mg/L)	Fe^{BH}	Polyvinyl alcohol-co-vinyl acetate-co-itaconic acid (PV3A) (5–10% by weight of NZVI)		$k_{obs} = 1.88$/h per 10 g/L of NZVI	98% removal after 3 h	Sun et al. (2007)
3	TCE (25 mg/L)	Commercial NZVI (100 nm)	–	Batch experiment using 0.1 g/L NZVI in DI water	$k_{obs} = 0.034$/h for 0.1 g/L NZVI	<10% removal in 120 min	He and Zhao (2005)
4	TCE (25 mg/L)	Commercial NZVI (100 nm)	Starch (either 0.2% (w/w) for 0.1 g/L Fe or 0.8% (w/w) for 1 g/L Fe solution)		$k_{obs} = 0.11$/h for 0.1 g/L NZVI or $k_{SA} = 0.02$ L/(h·m^2)	20% removal in 120 min	He and Zhao (2005)
5	TCE (20 mg/L)	Pd/Fe^{BH}	–	Batch experiment using 20 g/L NZVI in DI water	$k_{SA} = 0.1$ L/(h·m^2)	100% removal in 0.25 h	Wang and Zhang (1997)
6	TCE (25 mg/L)	Commercial NZVI with Pd (0.1% wt) (100 nm, Argonide, Sanford, FL)	–	Batch experiment using 1 g/L NZVI in DI water	$k_{obs} = 0.0016$/h for 1 g/L NZVI	<20% removal in 120 min	He and Zhao (2005)
7	TCE (4.4–290 mg/L)	RNIP (Fe^{H2})	–	Batch experiment in DI water at 0.35 g/L to 1.9 g/L NZVI	$k_{SA} = 4 \times 10^{-4}$ L/(h·m^2) for iron limited condition (0.35 g/L) and $k_{SA} = 3 \times 10^{-3}$	75% removal in 8 days	(Liu et al. 2005b)

(continued)

Table 3.1 (continued)

No.	Contaminant (initial concentration)	Type of particle	Dispersant or supported material	Experimental condition	Rate constant (pseudo-first order)	Contaminant removal (%)	References
					L/(h·m^2) for iron excess (1.9 g/L)		
8	TCE (4.4–290 mg/L)	Fe^{BH}	–		$k_{SA} = 2 \times 10^{-3}$ L/(h·m^2) for iron limited condition (0.35 g/L) and $k_{SA} = 1.4 \times 10^{-2}$ L/(h·m^2) for iron excess (1.9 g/L)	70–80% removal in less than 2 days	Liu et al. (2005b)
9	TCE (5.25 mg/L)	RNIP (Fe^{H2})	Poly(styrene sulfonate) (MW = 70 K) (adsorbed mass = 2.06 mg/m^2 of NZVI)	Batch experiment in 1 mM NaHCO3 at 2.8 g/L NZVI	$k_{SA} = 0.73 \pm 0.03 \times 10^{-3}$ L/(h·m^2)	90% removal in 160 h	Phenrat et al. (2009b)
10	TCE (5.25 mg/L)	RNIP (Fe^{H2})	Poly(styrene sulfonate) (MW = 1 M) (adsorbed mass = 1.92 mg/m^2 NZVI)		$k_{SA} = 0.44 \pm 0.04 \times 10^{-3}$L/(h·m^2)	–	Phenrat et al. (2009b)
11	TCE (5.25 mg/L)	RNIP (Fe^{H2})	Carboxymethylcellulose (MW = 90 K) (adsorbed mass = 0.98 mg/m^2 of NZVI)		$k_{SA} = 0.31 \pm 0.02 \times 10^{-3}$ L/(h·m^2)	–	Phenrat et al. (2009b)
12	TCE (5.25 mg/L)	RNIP (Fe^{H2})	Carboxymethylcellulose (MW = 700 K) (adsorbed mass = 2.03 mg/m^2 of NZVI)		$k_{SA} = 0.38 \pm 0.03 \times 10^{-3}$ L/(h·m^2)	–	Phenrat et al. (2009b)
13	TCE (5.25 mg/L)	RNIP (Fe^{H2})	Polyaspartate (MW = 2.5 K) (adsorbed		$k_{SA} = 0.15 \pm 0.01 \times 10^{-3}$ L/(h·m^2)	–	Phenrat et al. (2009b)

			mass = 2.29 mg/m^2 of NZVI)				
14	TCE (5.25 mg/L)	RNIP (Fe^{H2})	Polyaspartate (MW = 10 K) (adsorbed mass = 2.29 mg/m^2 of NZVI)		$k_{SA} = 0.14 \pm 0.01 \times 10^{-3}$ L/(h·m^2)	–	Phenrat et al. (2009b)
15	TCE (50 mg/L)	Pd/Fe^{BH} (Pd loading 0.1% wt)	–	Batch experiment in DI with iron dose of 0.1 g/L	$k_{obs} = 0.44$/h. per 0.1 g/L of Pd/Fe	40% removal after 120 min	He et al. (2007)
16	TCE (50 mg/L)	Pd/Fe^{BH} (Pd loading 0.1% wt)	CMC (0.2% (w/w))	Batch experiment using 0.1 g/L NZVI in DI water	$k_{obs} = 7.4$/h. per 0.1 g/L of Pd/Fe	Complete reduction after 40 min	He et al. (2007)
17	TCE (25 mg/L)	Pd/Fe^{BH} (Pd loading 0.1% wt)	–	Batch experiment using 0.1 g/L NZVI in DI water Batch experiment in DI with iron dose of 0.1 g/L	$k_{obs} = 0.0125$/h for 0.1 g/L NZVI	80% removal	He and Zhao (2005)
18	TCE (25 mg/L)	Pd/Fe^{BH} (Pd loading 0.1% wt)	Starch (either 0.2% (w/w) for 0.1 g/L Fe or 0.8% (w/w) for 1 g/L Fe solution)		$k_{obs} = 3.7$/h for 0.1 g/L NZVI or $k_{SA} = 0.67$ L/(h·m^2)	98% removal	He and Zhao (2005)
19	TCE (30 mg/L)	Fe^{H2} (using H_2 at 500 °C)	Activated carbon ($d_{50} = 0.8$ μm) (NZVI loading = 11%-20% wt)	Batch experiment at 1 g/L of NZVI and pH = 8.5 in DI water with 0.2 M NH_4Cl/NH_3- or $NaHCO_3$ buffer	$k_{obs} = 0.9$ to 4.2×10^{-2}/h or $k_{SA} = 0.6$ to 2.7×10^{-3} L/(h·m^2)	90% removal in 100 h	Mackenzie et al. (2012)

(continued)

Table 3.1 (continued)

No.	Contaminant (initial concentration)	Type of particle	Dispersant or supported material	Experimental condition	Rate constant (pseudo-first order)	Contaminant removal (%)	References
20	Tetrachloroethylene (PCE) (37 mg/L)	RNIP (Fe^{H2})	–	Batch experiment in 5 mM NaHCO3 and 10 g/L NZVI	$k_{SA} = 7.6 \times 10^{-4}$ L/(h·m^2)	Complete removal in 2.5 days	Fagerlund et al. (2012)
21	PCE (4.8 mg/L)	MRNIP2 (Fe^{H2})	Poly(maleic acid-co-olefin) (MW = 12 K)	Batch experiment in 5 mM NaHCO3 and various NZVI concentrations from 1 to 20 g/L	k_{SA} from 2×10^{-4} to 4×10^{-4} L/(h·m^2)	Complete removal in 50 h	(Kim et al. 2017)
22	PCE (20 mg/L)	Pd/Fe^{BH} (Pd loading 0.1% wt)	–	Batch experiment in DI water at 5 g/L NZVI	$k_{SA} = 12.2 \pm 0.36 \times 10^{-3}$ L/(h·m^2)	Complete removal in 1.5 h	Lien and Zhang (2001)
23	TCE (20 mg/L)	Pd/Fe^{BH} (Pd loading 0.1% wt)	–		$k_{SA} = 18.2 \pm 1.18 \times 10^{-3}$ L/(h·m^2)	Complete removal in 1.5 h	Lien and Zhang (2001)
24	tran-1,2-Dichloroethylene (t-DCE) (20 mg/L)	Pd/Fe^{BH} (Pd loading 0.1% wt)	–		$k_{SA} = 15.1 \pm 2.08 \times 10^{-3}$ L/(h·m^2)	Complete removal in 1.5 h	Lien and Zhang (2001)
25	cis-1,2-Dichloroethylene (c-DCE) (20 mg/L)	Pd/Fe^{BH} (Pd loading 0.1% wt)	–		$k_{SA} = 17.6 \pm 1.34 \times 10^{-3}$ L/(h·m^2)	Complete removal in 1.5 h	(Lien and Zhang 2001)
26	1,1-Dichloroethylene (1,1-DCE) (20 mg/L)	Pd/Fe^{BH} (Pd loading 0.1% wt)	–		$k_{SA} = 11.5 \pm 1.25 \times 10^{-3}$ L/(h·m^2)	Complete removal in 1.5 h	Lien and Zhang (2001)

Chlorinated ethane							
27	Hexachloroethane (HCA) (23.6 mg/L)	Fe^{BH}	–	Batch experiment in DI water in NZVI concentration of 0.08 g/L at the initial pH 7.2 to 7.8	$k_{obs} = 1.73 \pm 0.12$/h. or $k_{SA} = 7.7 \pm 0.7 \times 10^{-1}$ L/(h·m^2)	>90% removal in 1.3 h	Song and Carraway (2005)
28	Pentachloroethane (PCA) (19.19 mg/L)	Fe^{BH}	–		$k_{obs} = 1.79 \pm 0.09$/h or $k_{SA} = 7.96 \pm 0.63 \times 10^{-1}$ L/(h·m^2)	>90% removal in 1.3 h	Song and Carraway (2005)
29	1,1,2,2-Tetrachloroethane (1,1,1,2-TeCA) (18.3 mg/L)	Fe^{BH}	–		$k_{obs} = 1.21 \pm 0.10$/h or $k_{SA} = 5.38 \pm 0.56 \times 10^{-1}$ L/(h·m^2)	–	Song and Carraway (2005)
30	1,1,2,2-TeCA (18.3 mg/L)	Fe^{BH}	–		$k_{obs} = 6.82 \pm 0.85 \times 10^{-2}$/h or $k_{SA} = 3.03 \pm 0.42 \times 10^{-2}$ L/(h·m^2)	90% removal in 55 h	Song and Carraway (2005)
31	1,1,1-Trichloroethane (1,1,1-TCA) (13.4 mg/L)	Fe^{BH}	–		$k_{obs} = 3.4 \pm 0.2 \times 10^{-1}$/h or $k_{SA} = 1.51 \pm 0.13 \times 10^{-1}$ L/(h·m^2)	80% removal in 5 h	Song and Carraway (2005)
32	1,1,2-Trichloroethane (1,1,2-TCA) (13.4 mg/L)	Fe^{BH}	–	Batch experiment in DI water in NZVI concentration of 0.08 g/L at the initial pH 7.2 to 7.8	$k_{obs} = 5.2 \pm 0.71 \times 10^{-3}$/h or $k_{SA} = 2.31 \pm 0.34 \times 10^{-3}$ L/(h·m^2)	50% removal in 110 h	Song and Carraway (2005)
33	1,1-Dichloroethane (1,1-DCA) (9.9 mg/L)	Fe^{BH}	–		$k_{obs} = 2.41 \pm 0.52 \times 10^{-4}$/h or $k_{SA} = 1.99 \pm 0.44 \times 10^{-5}$ L/(h·m^2)	–	Song and Carraway (2005)
34	1,2-Dichloroethane (1,2-DCA) (9.9 mg/L)	Fe^{BH}	–		$k_{obs} < 5 \times 10^{-5}$/h or $k_{SA} = 4 \times 10^{-6}$ L/(h·m^2)	–	Song and Carraway (2005)
35	HCA (20–30 mg/L)	Pd/Fe^{BH} (Pd loading 0.5% wt)	–	Batch experiment in DI	$k_{obs} = 3.43$/h		

(continued)

Table 3.1 (continued)

No.	Contaminant (initial concentration)	Type of particle	Dispersant or supported material	Experimental condition	Rate constant (pseudo-first order)	Contaminant removal (%)	References
				water in NZVI concentration of 5 g/L		100% removal in 1.7 h	Lien and Zhang (2005)
36	PCA	Pd/Fe^{BH} (Pd loading 0.5% wt)	–		$k_{obs} = 4.46$/h	–	(Lien and Zhang 2005)
37	1,1,1,2-TeCA	Pd/Fe^{BH} (Pd loading 0.5% wt)	–		$k_{obs} = 3.60$/h	–	Lien and Zhang (2005)
38	1,1,1,2-TeCA	Pd/Fe^{BH} (Pd loading 0.5% wt)	–		$k_{obs} = 1.51$/h	–	Lien and Zhang (2005)
39	1,1,1-TCA	Pd/Fe^{BH} (Pd loading 0.5% wt)	–		$k_{obs} = 0.93$/h	100% removal in 7 h	Lien and Zhang (2005)
Chlorinated methane							
40	Tetrachloromethane (or carbon tetrachloride (CT) (0.6 mg/L)	RNIP (Fe^{H2}) (surface area = 29 m^2/g)	–	Batch experiment in DI water in various NZVI concentrations	$k_{SA} = 1.2 \times 10^{-2}$ to 1.5×10^{-1} L/(h·m^2)	–	Nurmi et al. (2005)
41	CT (0.6 mg/L)	Fe^{BH} (surface area = 33.5 m^2/g)	–		$k_{SA} = 4.2 \times 10^{-2}$ to 3.0×10^{-1} L/(h·m^2)	–	Nurmi et al. (2005)
42	CT (0.6 mg/L)	Fe^{El} (surface area = 0.12 m^2/g)	–		$k_{SA} = 0.12$–2.4 L/(h·m^2)	–	Nurmi et al. (2005)

43	CT (30 mg/L)	Fe^{BH}	–	Batch experiment in DI water (pH 7.5) at 0.16 g/L NZVI	$k_{obs} = 5.02 \pm 0.44$/h $k_{SA} = 1.12 \pm 0.11$ L/(h·m^2)	100% removal in 1.5 h	Song and Carraway (2006)
44	Trichloromethane (or chloroform (CF) (11.9 mg/L)	Fe^{BH}	–		$k_{obs} = 1.89 \pm 0.18 \times 10^{-1}$/h $k_{SA} = 4.20 \pm 0.47 \times 10^{-2}$ L/(h·m^2)	80% removal in 10 h	Song and Carraway (2006)
45	CT (15.9 mg/L)	Fe^{BH}	–	Batch experiment in DI water at 12.5 g/L NZVI	$k_{SA} = 5.31 \times 10^{-4}$ L/(h·m^2)	100% removal in 20 h	Lien and Zhang (1999)
46	CT (15.9 mg/L)	Pd/Fe^{BH} (Pd loading is 0.06% wt)	–		$k_{SA} = 9.0 \times 10^{-3}$ L/(h·m^2)	100% removal in 1 h	Lien and Zhang (1999)
47	CF (14.8 mg/L)	Fe^{BH}	–		$k_{SA} = 8.41 \times 10^{-5}$ L/(h·m^2)	> 95% removal in 100 h	Lien and Zhang (1999)
48	CF (14.8 mg/L)	Pd/Fe^{BH} (Pd loading is 0.06% wt)	–		$k_{SA} = 6.5 \times 10^{-3}$ L/(h·m^2)	>95% removal in 1 h	Lien and Zhang (1999)
Chlorinated and aromatic nitro hydrocarbon							
49	Hexachlorobenzene (HCB)	Fe^{BH}	–	Batch experiment in DI with NZVI of 133 g/L at pH = 8	$k_{obs} = 0.14$/h	60% removal in 24 h	Shih et al. (2009)
50	HCB	Pd/Fe^{BH} (Pd loading is 0.02% wt)	–	Batch experiment in DI with NZVI of 133 g/L at pH = 8	$k_{obs} = 0.23$/h	70% removal in 24 h	Shih et al. (2009)
51	HCB (0.2 mg/L)	Cu/Fe (cu loading = 5% wt)	–	Batch experiment in DI with	$k_{obs} = 0.056 \pm 0.008$/h	98% removal in 3 h	Zhu et al. (2010)

(continued)

Table 3.1 (continued)

No.	Contaminant (initial concentration)	Type of particle	Dispersant or supported material	Experimental condition	Rate constant (pseudo-first order)	Contaminant removal (%)	References
52	HCB (0.2 mg/L)	Fe	–	NZVI of 40 g/L at pH = 4	$k_{obs} = 0.012 \pm 0.003$/h	88% removal in 192 h	Zhu et al. (2010)
53	Nitrobenzene (NB) (20 mg/L)	Fe^{H2}	–	Batch experiment at 1 g/L of NZVI	$k_{obs} = 9.30 \pm 2.13$/h for NZVI	56% removal for NZVI	Zhang et al. (2013)
54	NB (20 mg/L)	Fe^{H2}	Ordered mesoporous materials, including platelet shape and short mesochannels (SBA-15_S) and conventional fibrous SBA-15 (SBA-15_L)	Batch experiment at 1 g/L of NZVI	$k_{obs} = 29.40 \pm 2.52$/h for NZVI/SBA-15_S and $k_{obs} = 37.50 \pm 4.18$/h for NZVI/SBA-15_L	94% removal for NZVI/SBA-15_S and 83.9% removal for NZVI/SBA-15_L in 12 h	Zhang et al. (2013)
55	1, 2, 4-trichloro-benzene (1,2,4-TCB) (25 mg/L)	Cu/Fe^{BH} (cu loading is 0.5% wt)	Carboxymethyl cellulose (MW = 90 K) (0.2–0.4% wt)	Batch experiment in DI water at 1 g/L NZVI	$k_{obs} = 0.06$–0.09/h	75–88% removal in 25 h	Cao et al. (2011)
56	1,2,4-TCB (19.2 mg/L)	Pd/Fe^{BH} (Pd loading is 0.1% wt)	SDS (1 critical micelle concentration (CMC))	Batch experiment in DI water at 0.71 g/L NZVI	$k_{obs} = 6.06 \pm 1.14$/h	100% removal in 60 min	Zhu et al. (2008)
57	1,2,4-TCB (19.2 mg/L)	Pd/Fe^{BH} (Pd loading is 0.1% wt)	NPE (1 CMC)		$k_{obs} = 9.18 \pm 1.86$/h	100% removal in 60 min	Zhu et al. (2008)
58	1,2,4-TCB (19.2 mg/L)	Pd/Fe^{BH} (Pd loading is 0.1% wt)	TX-100 (1 CMC)		$k_{obs} = 5.64 \pm 1.44$/h	100% removal in 60 min	Zhu et al. (2008)
59	1,2,4-TCB (19.2 mg/L)	Pd/Fe^{BH} (Pd loading is 0.1% wt)	CTAB (1 CMC)		$k_{obs} = 13.9\,8 \pm 1.62$/h	100% removal in 60 min	Zhu et al. (2008)

60	1,2,4-TCB (19.2 mg/L)	Pd/Fe^{BH} (Pd loading is 0.1% wt)	DCP (1 CMC)	Batch experiment in DI water at 0.71 g/L NZVI	$k_{obs} = 0.9 \pm 0.48$/h	100% removal in 60 min	Zhu et al. (2008)
61	1,2,4-TCB (19.2 mg/L)	Pd/Fe^{BH} (Pd loading is 0.1% wt)	Natural organic matter (NOM) (10 mg/L)		$k_{obs} = 3.54 \pm 0.78$/h	30% removal in 60 min	Zhu et al. (2008)
62	1,2,4-TCB (19.2 mg/L)	Pd/Fe^{BH} (Pd loading is 0.1% wt)	NOM (50 mg/L)		$k_{obs} = 0.54 \pm 0.42$/h	–	Zhu et al. (2008)
63	1,2,4-TCB (19.2 mg/L)	Pd/Fe^{BH} (Pd loading is 0.1% wt)	NOM (200 mg/L)		$k_{obs} = 0.18 \pm 0.06$/h	–	Zhu et al. (2008)
64	1,2,4-TCB (30.8 mg/L)	Pd/Fe^{BH} (Pd loading is 0.1–1% wt)	Chitosan (3.33 g/L)	Batch experiment in DI water at 1.65 g/L NZVI	$k_{obs} = 5.87$/h	100% removal in 60 min	Zhu et al. (2006)
65	1,2,4-TCB (30.8 mg/L)	Pd/Fe^{BH} (Pd loading is 0.1–1% wt)	Silica (3.33 g/L)		$k_{obs} = 1.86$/h	95% removal in 120 min	Zhu et al. (2006)
66	Para-nitrochlorobenzene (p-NCB) (40 mg/L)	Ni/Fe^{BH} (Ni loading is 2% wt)	–	Batch experiment in DI water at 6 g/L NZVI at pH = 7	$k_{obs} = 2.39$/h	100% removal in 300 min	Xu et al. (2009)
67	Pentachlorophenol (PCP) (0.075 mM)	Fe^{BH} (Fe^0 = 2.95% on the weight basis of clay)	2% Smectite clay in the suspension	Batch experiment in DI water at pH = 9	$k_{obs} = 0.001$/h	20% removal in 14 days	Jia and Wang (2015)
68	PCP (0.075 mM)	Pd/Fe^{BH} (Fe^0:Pd^0 = 2.95%:0.065% on the weight basis of clay)	2% Smectite clay in the suspension	Batch experiment in DI water at pH = 9	$k_{obs} = 0.487$/h	95% removal in 6 h	(Jia and Wang 2015)
69	2,3,4,5-TeCP and 2,3,4,6-TeCP and 2,3,5,6-TeCP (0.075 mM) (TeCP = Tetrachlorophenol)	Pd/Fe^{BH} (Fe^0:Pd^0 = 2.95%:0.065% on the weight basis of clay)	2% Smectite clay in the suspension	Batch experiment in DI water at pH = 9	$k_{obs} = 0.502$–0.586/h	–	Jia and Wang (2015)
70		Pd/Fe^{BH} (Fe^0:Pd^0 = 2.95%:0.065% on	2% Smectite clay in the suspension		$k_{obs} = 0.968$–1.064/h	–	

(continued)

Table 3.1 (continued)

No.	Contaminant (initial concentration)	Type of particle	Dispersant or supported material	Experimental condition	Rate constant (pseudo-first order)	Contaminant removal (%)	References
	2,3,4-TCP and 2,3,6-TCP and 2,4,6-TCP (0.075 mM) (TCP is Trichlorophenol)	the weight basis of clay)		Batch experiment in DI water at pH = 9			Jia and Wang (2015)
71	3,4,5-TCP and 2,4,5-TCP and 2,3,5-TCP (0.075 mM)	Pd/Fe^{BH} (Fe^0:Pd^0 = 2.95%:0.065% on the weight basis of clay)	2% Smectite clay in the suspension	Batch experiment in DI water at pH = 9	k_{obs} = 1.300–1.459/h	–	Jia and Wang (2015)
72	2,6-Dichlorophenol (2,6-DCP) (0.075 mM)	Pd/Fe^{BH} (Fe^0:Pd^0 = 2.95%:0.065% on the weight basis of clay)	2% Smectite clay in the suspension	Batch experiment in DI water at pH = 9	k_{obs} = 1.912/h	–	Jia and Wang (2015)
73	3,5-Dichlorophenol (3,5-DCP) (0.075 mM)	Pd/Fe^{BH} (Fe^0:Pd^0 = 2.95%:0.065% on the weight basis of clay)	2% Smectite clay in the suspension	Batch experiment in DI water at pH = 9	k_{obs} = 2.139/h	–	Jia and Wang (2015)
74	2,3-DCP and 2,4-DCP and 3,4-DCP (0.075 mM)	Pd/Fe^{BH} (Fe^0:Pd^0 = 2.95%:0.065% on the weight basis of clay)	2% Smectite clay in the suspension	Batch experiment in DI water at pH = 9	k_{obs} = 2.234–2.351/h	–	Jia and Wang (2015)
75	2,5-DCP (0.075 mM)	Pd/Fe^{BH} (Fe^0:Pd^0 = 2.95%:0.065% on the weight basis of clay)	2% Smectite clay in the suspension	Batch experiment in DI water at pH = 9	k_{obs} = 3.265/h	–	Jia and Wang (2015)
76	4-CP and 2-CP (0.075 mM) (CP is chlorophenol)	Pd/Fe^{BH} (Fe^0:Pd^0 = 2.95%:0.065% on the weight basis of clay)	2% Smectite clay in the suspension	Batch experiment in DI water at pH = 9	k_{obs} = 8.606–9.603/h	–	Jia and Wang (2015)

77	3-CP (0.075 mM)	Pd/Fe^{BH} (Fe^0:Pd^0 = 2.95%:0.065% on the weight basis of clay)	2% Smectite clay in the suspension	Batch experiment in DI water at pH = 9	k_{obs} = 15.63/h	–	Jia and Wang (2015)
Chlorinated biphenyl							
78	Polychlorinated biphenyls (PCBs) (2.5 mg/L)	Pd/Fe^{BH} (Pd loading 0.1% wt)	–	Batch experiment using 0.1 g/L NZVI in DI water	$k_{obs} = 2.9 \times 10^{-3}$/h for 0.1 g/L NZVI	20% removal in 100 h	He and Zhao (2005)
79	PCBs (2.5 mg/L)	Pd/Fe^{BH} (Pd loading 0.1% wt)	Starch (either 0.2% (w/w) for 0.1 g/L Fe or 0.8% (w/w) for 1 g/L Fe solution)	Batch experiment using 0.1 g/L NZVI in DI water	k_{obs} = 0.017/h for 0.1 g/L NZVI	80% removal in 100 h	He and Zhao (2005)
80	2-Chlorobiphenyl (4 mg/L)	Pd/Fe^{BH} (0.68% Pd to 14.4% Fe)	Granular activated carbon (GAC)	Batch experiment in DI water at 100 g/L of GAC embedded with Pd/FeBH	Not determined due to complex sorption and dechlorination processes	1.16% removal after 2 days. The residual was adsorbed on the surface of GAC	Choi et al. (2008)
81	2-Chlorobiphenyl (4 mg/L)	Fe^{BH}	Granular activated carbon (GAC)		Not determined due to complex sorption and dechlorination processes	90% removal after 2 days. The residual was adsorbed on the surface of GAC	Choi et al. (2008)
Halogenated bisphenol A (flame retardant)							
82	Tetrabromobisphenol A (10 mg/L)	Ni/Fe^{BH} (Ni loading = 0.5% wt)	–	Batch experiment in DI water at 3 g/L NZVI and	k_{obs} = 2.7/h or $k_{SA} = 3.3 \times 10^{-2}$ L/(h·m^2)	Successfully degraded within 2 h	Li et al. (2016)

(continued)

Table 3.1 (continued)

No.	Contaminant (initial concentration)	Type of particle	Dispersant or supported material	Experimental condition	Rate constant (pseudo-first order)	Contaminant removal (%)	References
				pH 5–6 (optimal)			
83	Tetrabromobisphenol A (16.30 mg/L)	Pd/Fe^{BH} (Pd loading = 0.022%)	–	Batch experiment in DI water at 4 g/L NZVI and pH 4.2	$k_{obs} = 138$/h	99% removal efficiency in 45 min	Huang et al. (2013)
84	Tetrachlorobisphenol A (10 mg/L)	Ni/Fe^{BH} (Ni loading = 0.5% wt)	–	Batch experiment in DI water at 2 g/L NZVI and pH 7	$k_{obs} = 0.57 \pm 0.02$/h	95% removal in 360 min	Li et al. (2017)
85	Tetrachlorobisphenol A (10 mg/L)	Fe^{BH}	–		$k_{obs} = 0.03$/h	12% removal in 360 min	Li et al. (2017)
86	Tetrabromobisphenol A) (10 mg/L)	Ni/Fe^{BH} (Ni loading = 0.5% wt)	–		$k_{obs} = 2.24 \pm 0.17$/h	95% removal in 120 min	Li et al. (2017)
87	Tetrabromobisphenol A) (10 mg/L)	Fe^{BH}	–		$k_{obs} = 0.08$/h	15% in 120 min	Li et al. (2017)
Explosives							
88	2,4,6-trinitrotoluene (TNT) (80 mg/L)	NZVI (powder)	–	Batch experiment in DI water at 5 g/L NZVI and pH 4	$k_{obs} = 0.31$/h	Completely degraded within 3 h	Zhang et al. (2010)
89	1,3,5-Trinitro-1,3,5-triazinane (RDX) (0.18 mg/L)	Fe^{BH}	–	Batch experiment in DI water at 0.3 g/L NZVI and pH 5	$k_{obs} = 1.14 \pm 0.12$/h	75% removal in 60 min	Naja et al. (2008)
90	RDX (0.18 mg/L)	Fe^{BH}	Poly(acrylic acid) (PAA) (61 g/L, degree of polymerization = 100)	Batch experiment in DI	$k_{obs} = 4.92 \pm 0.12$/h	100% removal in 60 min	Naja et al. (2008)

91	RDX (0.18 mg/L)	Fe^{BH}	Carboxymethyl cellulose (CMC) (0.5% wt, degree of polymerization = 100)	water at 0.3 g/L NZVI and pH 5	$k_{obs} = 48.96 \pm 4.02$/h	100% removal in 5 min	Naja et al. (2008)
Dye, pesticides, and others							
92	Acid blue 113 dye azo dye solution	Fe^{BH}	Resin (NZVI loads of 4.9–50.8 mg/g)	Batch experiment with 20 g/L of resin imbedded NZVI and 50–600 mg/L acid blue 113	$k_{obs} = 8.22$–45.36/h by NZVI loads of 4.9–50.8 mg/g	Almost 100% dye removal and 12.6% TOC removal after 30 min	Shu et al. (2010)
93	Methyl orange (MO) dye	Fe^{BH}	Bentonite	Batch experiment at 1 g/L of bentonite-supported NZVI and 100–800 mg/L of MO	$k_{obs} = 2.04$/h at MO concentration of 800 mg/L to 6.48/h at 100 mg/L MO	79.46% removal after 10 min and Nearly 100% after 30 min	Chen et al. (2011b)
94	Methylene blue (MB) dye	Fe^{BH}	Palygorskite	Batch experiment at 1 g/L of palygorskite-supported NZVI 100 mg/L MB at a natural pH	–	89.36% in 30–60 min	Frost et al. (2010)
95	MO (60 mg/L)	Fe^{BH}	Biochar NZVI/BC (1:3, 1:5, or 1:7 by wt)	Batch experiment in DI water at 0.6–0.9 g/L biochar	$k_{obs} = 28.56$–44.58/h	93.3–98.5% removal in 25 min	Han et al. (2015)

(continued)

Table 3.1 (continued)

No.	Contaminant (initial concentration)	Type of particle	Dispersant or supported material	Experimental condition	Rate constant (pseudo-first order)	Contaminant removal (%)	References
				supported NZVI at pH 4.06–9.13			
96	2,4-dichloro-phenoxyacetic acid (10 mg/L)	Pd/Fe^{BH} (Pd loading = 0.8% wt)	–	Batch experiment in DI water at 0.6 g/L NZVI and pH 6	$k_{obs} = 8.42$/h	25% within 180 min	Zhou et al. (2011)
97	2,4-dichloro-phenoxyacetic acid (10 mg/L)	Pd/Fe^{BH} (Pd loading = 0.8% wt)	Carboxymethyl cellulose (CMC) (CMC/Fe, (wt/wt)) = 2/1 to 10/1)		k_{obs} = 5.03/h, 3.70/h, 8.91/h for CMC/Fe = 2/1, 10/1, and 5/1, respectively	45%, 80%, and 97% within 180 min for CMC/Fe = 2/1, 10/1, and 5/1, respectively	Zhou et al. (2011)
98	Alachlor [2-chloro-20,60-diethyl-N-(methoxymethyl) acetanilide] (10–40 mg/L)	Fe^{BH}	–	Batch experiment in DI water at 4 g/L NZVI and pH 7–8.5	$k_{SA} = 38.5 \times 10^{-5}$ L/(h·m^2)	92%–96% after 72 h and completely reduced after 5 days	Thompson et al. (2010)
99	Benzoquinone (21–210 mg/L)	RNIP (Fe^{H2}) (surface area = 29 m^2/g)	–	Batch experiment in DI water in various NZVI concentrations	$k_{SA} = 1.8 \times 10^{-2}$ to 1.2×10^{-1} L/(h·m^2)	–	Nurmi et al. (2005)
100	Benzoquinone (21–210 mg/L)	Fe^{BH} (surface area = 33.5 m^2/g)	–	Batch experiment in DI water in	k_{SA} = 0.6–3 L/(h·m^2)	–	Nurmi et al. (2005)

				various NZVI concentrations			
101	Benzoquinone (21–210 mg/L)	Fe^{El} (surface area = 0.12 m^2/g)	–	Batch experiment in DI water in various NZVI concentrations	$k_{SA} = 6 \times 10^{-2}$ to 3.6 L/(h·m^2)	–	Nurmi et al. (2005)
102	γ-Hexachlorocyclohexane (7.5 mg/L)	Fe^{BH}	–	Batch experiment in DI water in various NZVI concentrations (from 0.015 to 0.39 g/L)	$k_{SA} = 1.5$ to 7.20×10^{-2} L/(h m^2)	100% removal in 24 h at NZVI concentration of 0.1–0.39 mg/L	Elliott et al. (2009)

Note: Fe^{BH} NZVI synthesized by borohydride reduction (see Chap. 2)
Fe^{H2} NZVI synthesized by H2 reduction (see Chap. 2)
RNIP and MRNIP2 Fe^{H2} distributed by Toda, Japan
k_{obs} observed rate constant
k_{SA} surface-area normalized rate constant

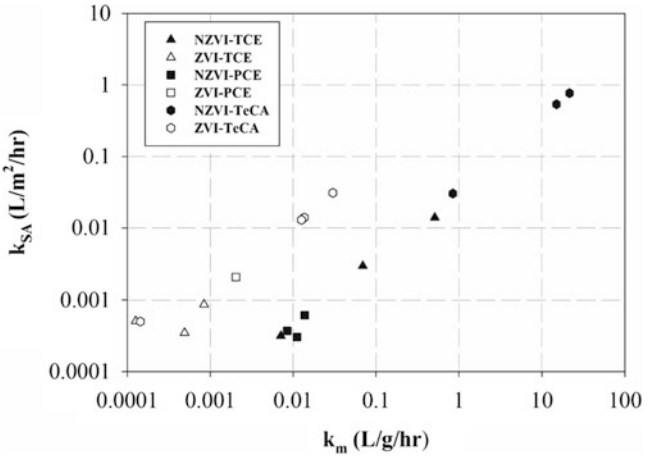

Fig. 3.1 Comparison of surface-area normalized rate constants (k_{SA}) against mass normalized rate constants (k_M) for the degradation of TCE, PCE, and TeCA by NZVI and bulk ZVI. (Data from Johnson et al. (1996), Liu et al. (2005b), Song and Carraway (2005), Amir and Lee (2011), Phenrat et al. (2016), Hepure Technology Inc. (2017), Kim et al. (2017))

CT by NZVI and bulk ZVI, the results show that NZVI gives larger k_M but similar k_{SA} values (Nurmi et al. 2005; Tratnyek and Johnson 2006). Nevertheless, when doing the same analysis for other contaminants, including trichloroethylene (TCE), tetrachloroethylene (PCE), and tetrachloroethane (TeCA) (Fig. 3.1), we found that a significant increase in k_{SA} for NZVI in comparison to ZVN was observed for TeCA and TCE but not for PCE. This suggests a potential "nano-effect," but it seems to be, at least in part, governed by the interaction between the contaminant and NZVI surface.

Regardless of its particle size and probable nano-effect, the fundamental chemistry of NZVI in an aqueous environment from a reaction viewpoint is the same as ZVI. For environmental remediation purposes, Fe^0 can be oxidized by halogenated organics (as electron acceptors) as long as such organics have an $E_H{}^0$ greater than −0.447 V. As a result of the electron transfer, in most cases, NZVI transforms such organic contaminants to more environmentally benign byproducts (Eqs. 3.1 and 3.2 using TCE as an example) (Liu et al. 2005a, b). In the meantime, Fe^0 can also react with water (or H^+) to produce H_2 gas (Eq. 3.3), which is a competing reaction to the dechlorination reaction and is strongly controlled by the availability of H^+ (i.e., pH).

$$Fe^{2+} + 2e^- \rightarrow Fe^0, \quad E_H{}^0 = -0.447 \text{ V} \tag{3.1}$$

$$TCE + ne^- + (n-3)H^+ \rightarrow \text{product} + 3Cl^- \tag{3.2}$$

$$H^+ + e^- \rightarrow H^* \rightarrow \frac{1}{2}H_2 \tag{3.3}$$

Although the oxidation of Fe^0 to Fe^{2+} (Eq. 3.1) is usually assumed, in environmentally relevant applications (i.e., groundwater at a natural pH), the transformation of Fe^0 to the film of iron oxide, such as magnetite (Fe_3O_4) (Eq. 3.4) and maghemite (Fe_2O_3), is often observed (Liu et al. 2005b; Reinsch et al. 2010). Thermodynamically, the Fe^0/Fe_3O_4 couple is more favorable than the Fe^0/Fe^{2+}couple at a pH above 6.1. The oxidation of Fe^0 to Fe_3O_4 provides an additional 2/3 mole of electrons per mole of Fe^0 oxidized in comparison to the oxidation to Fe^{2+} (Liu et al. 2005b). However, the formation of iron oxide film can passivate NZVI and adversely affect its reactivity and reactive life time (Liu et al. 2005b; Reinsch et al. 2010).

$$Fe_3O_4 + 8H^+ + 8e^- \rightarrow 3Fe^0 + 4H_2O \tag{3.4}$$

As shown in Eqs. 3.1, 3.2, 3.3, and 3.4, electrons from the NZVI oxidation can be used to reduce contaminants or to produce H_2. For bimetallic NZVI (i.e., NZVI modified by noble metals, such as Pd, Pt, and Rh; (Wang and Zhang 1997; Zhang et al. 1998) and highly disordered monometallic NZVI (Liu et al. 2005a); see Sect. 3.1.3.1), H_2 can be activated and used for dechlorination via hydrodechlorination (Eq. 3.5).

$$H_2(g) \leftrightarrow 2H_{ad} \leftrightarrow 2H^+_{(aq)} + 2e^- \tag{3.5}$$

This explains the database in Table 3.1, in that bimetallic NZVI is typically 10–50 times more reactive than bare NZVI for the same contaminant, considering the enhanced pseudo-first-order reaction rate constant. The cost-effectiveness of in situ remediation using NZVI can be substantially affected by how electrons are utilized. In addition, the ability to utilize H_2 for hydrodechlorination and the characteristics of the iron oxide film formed on the surface of NZVI influence its lifetime, reactivity, and thus treatment efficiency. For NZVI, these phenomena are controlled by (1) intrinsic properties of the materials and (2) environmental conditions where NZVI particles are applied. These factors will be discussed later in this chapter, but we will first discuss reductive degradation pathways of various kinds of contaminants in aqueous environments in Sect. 3.1.2.

3.1.1 Reductive Transformation Pathways

3.1.1.1 Chlorinated Methane

While chlorinated methane, such as tetrachloromethane (or carbon tetrachloride (CT)) and trichloromethane (or chloroform (CF)), are mendable by NZVI, dichloromethane (DCM) shows negligible reactivity toward NZVI, giving the reactivity order of

CT > chloroform (CF) >> DCM (Song and Carraway 2006); Table 3.1). Nevertheless, the reductive transformation of CT using NZVI (both Fe^{BH} and Fe^{H2}) cannot completely dechlorinate CT to methane. Instead, it produces toxic byproducts including CF (18.4–39.3% of the initial concentration of CT) and dichloromethane (0–2.4% of the initial concentration of CT) as well as unknown byproducts (23.3–42.5% of the initial concentration of CT) presumably methane, carbon monoxide, and formate, while CT retains 15.8–58.2% of its initial concentration after 27 h (see Table 3.1) (Nurmi et al. 2005; Song and Carraway 2006). Because the dechlorination reactions are heterogeneous, the rates depend greatly on the interaction between chlorinated organics and the NZVI surface (iron oxide). For dechlorination of highly chlorinated organics such as CT, CF, and DCM, stepwise electron transfer takes place. The weak sorption of chlorinated methane on the NZVI surface may result in a short residence time and desorption of incompletely dechlorinated compounds. Interestingly, while Fe^{BH} was reported to perform indirect dechlorination of chlorinated ethene using reactive hydrogen species (Liu et al. 2005a), for chlorinated methane, the dechlorination occurs via a direct electron transfer reduction mechanism, rather than the indirect mechanism (Song and Carraway 2006).

Two possible dechlorination pathways include hydrogenolysis and α elimination. Hydrogenolysis is a two-step electron transfer reaction initiated by direct dissociative electron transfer, in which the first electron addition results in dissociation of the molecule to a trichloromethyl free radical ($\bullet CCl_3$) and chloride (Mccormick and Adriaens 2004). The free radical can subsequently form CF through the direct abstraction of hydrogen (Fig. 3.2a) or could be further reduced to a trichloromethyl carbanion ($:CCl_3$), which then forms CF via the rapid addition of H^+ from the solution (Mccormick and Adriaens 2004; Song and Carraway 2006) (Fig. 3.2a). This is supposed to be a prevalent pathway of CT degradation by NZVI, given that CF is a major byproduct of the degradation. Similarly, hydrogenolysis is supposed to be a major degradation pathway for CF as well, given that DCM is the major byproduct (Fig. 3.2b) (Song and Carraway 2006).

On the other hand, CH_4 was also observed along with DCM in the reduction of CT and CF. Since DCM is a rather inert intermediate, the sequential hydrogenolysis of DCM to CH_4 is unlikely. Consequently, methane formation must be caused by a parallel CT degradation pathway, bypassing CF and DCM as an intermediate. This can happen via concerted reductive elimination steps (two-electron transfer (α elimination) and four-electron transfer, respectively) to form dichloromethylene, methylene, and eventually methane (Fig. 3.2c). Notedly, α elimination is a dichloro-elimination process involving a two-electron transfer to the molecule and the elimination of two chlorine atoms. The reaction products are less-saturated aliphatic hydrocarbons and two chloride ions.

Notedly, α elimination is the elimination of chlorine atoms from one carbon atom, while β elimination occurs when chlorine atoms are removed from two different carbons. Reductive β elimination is known to be a preferential pathway for compounds possessing (α, β) pairs of chlorine atoms (Arnold and Roberts 2000), while hydrogenolysis or reductive α elimination is the primary transformation pathway for compounds possessing only α chlorines (Mccormick and Adriaens 2004; Song and Carraway 2005).

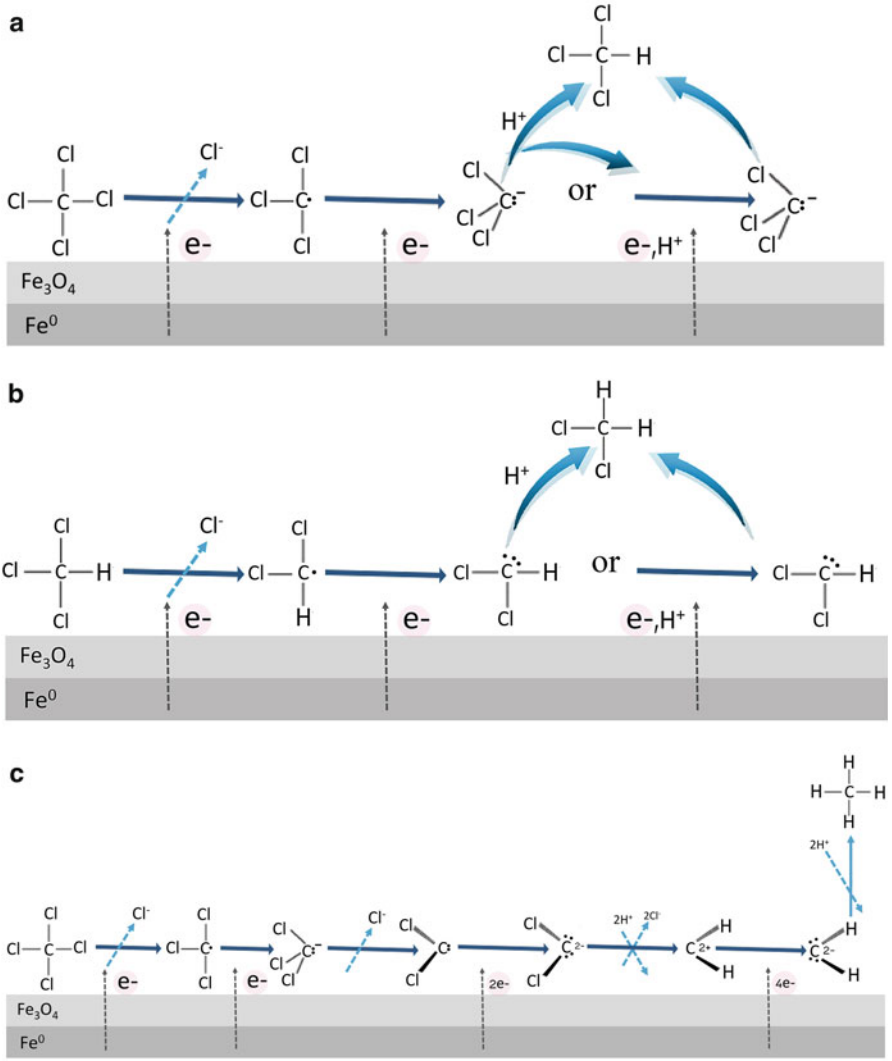

Fig. 3.2 (**a**) CT degradation pathway forming CF via trichloromethyl radical or carbanion intermediates, (**b**) CF degradation pathway forming DCM via dichloromethyl radical or carbanion intermediates, and (**c**) speculated methane (CH_4) formation pathway from the dichlorocarbene intermediate to CH_4 involving multi-electron transfers. (Adapted from Mccormick and Adriaens (2004), Song and Carraway (2006))

3.1.1.2 Chlorinated Ethene and Ethane

The NZVI can completely dechlorinate all chlorinated ethene and ethane (except 1,2-DCA) to non-chlorinated intermediates, such as acetylene, and byproducts including ethene and ethane. Unlike chlorinated methane, the main degradation pathway of chlorinated ethenes via NZVI is dichloro-elimination (β elimination)

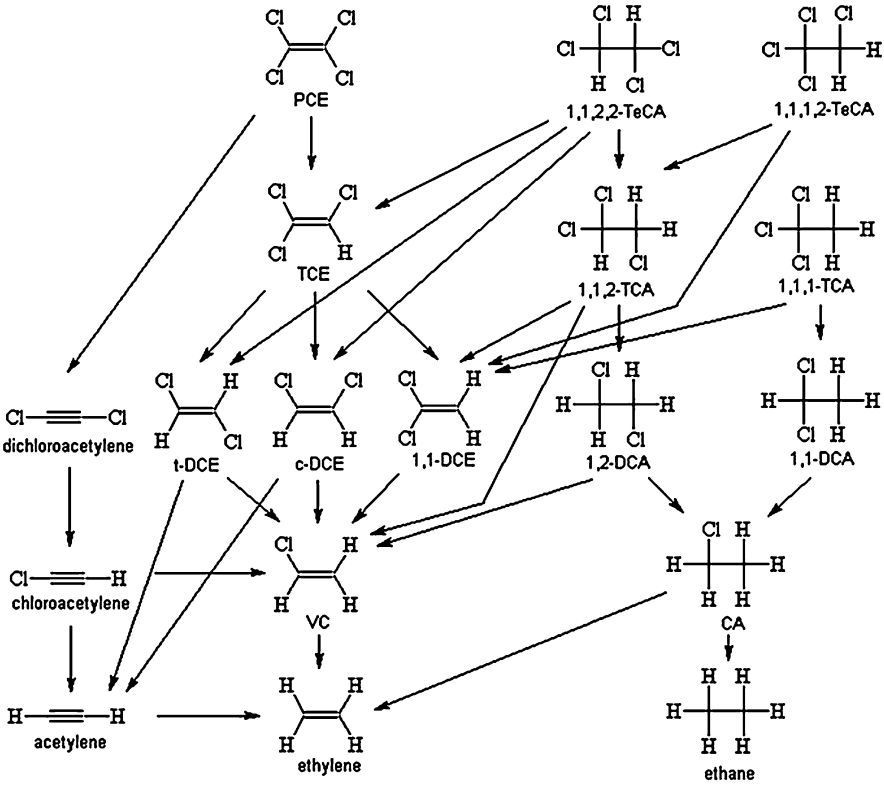

Fig. 3.3 Dechlorination pathway, ethene and ethane (Tobiszewski and Namieśnik 2012). (Reprinted with permission from Tobiszewski and Namieśnik (2012). Copyright (2012) Springer Nature)

followed by hydrogenolysis (Fig. 3.3). Similarly, the main degradation pathways of chlorinated ethane, such as HCA, PCA, and 1,1,1,2-TeCA, via NZVI is β elimination followed by hydrogenolysis (Fig. 3.3). Nevertheless, for 1,1,2,2-TeCA and both 1,1,1-TCA and 1,1,2-TCA, dehydrohalogenation becomes equally important, if not more important, than β elimination, especially at high a pH (Song and Carraway 2005).

Fundamentally, for chlorinated ethene, β elimination is preferable over hydrogenolysis because thermodynamic reduction potentials for two-electron reduction of chlorinated ethene and ethane via β elimination are more favorable than hydrogenolysis. This is demonstrated by an example of the half reaction of PCE transformation via β elimination (Eq. 3.6) and hydrogenolysis (Eq. 3.7) (Totten and Roberts 2010). From a kinetic viewpoint, the predominance of β elimination over hydrogenolysis is also partially due to the rapidity of intermolecular rearrangements (leading to β elimination) compared to bimolecular collisions with H^+ (leading to hydrogenolysis) at moderately basic pHs (Arnold and Roberts 2000).

$$CCl_2 = CCl_2 + 2e^- \rightarrow CCl \equiv CCl + 2Cl^- \quad E_H^0 = 0.631 \text{ V} \tag{3.6}$$

$$CCl_2 = CCl_2 + 2e^- + H^+ \rightarrow CCl_2 = CHCl + Cl^- \quad E_H^0 = 0.592 \text{ V} \tag{3.7}$$

Additionally, Fe^{BH} was reported to perform indirect dechlorination of chlorinated ethene using reactive hydrogen species (Liu et al. 2005a). This will be discussed in more detail in the next section.

Since the rate-limiting step in the reduction of chlorinated ethene and ethane using ZVI is supposed to be the transfer of a single electron and the formation of an alkyl radical (Johnson et al. 1996; Arnold and Roberts 2000), Scherer et al. (1998) proposed linear free energy relationships (LFERs) capable of explaining or predicting the rates of dehalogenation by ZVI. They showed that, at the same number of chlorine atoms, dechlorination rate constants of chlorinated ethanes are typically higher than chlorinated ethene. For an internal comparison among chlorinated ethene or among chlorinated ethane, the dechlorination rate constants tend to increase with increasing chlorination of the compounds. As for NZVI, the reactivity of chlorinated ethanes summarized in Table 3.1 reasonably agrees with this trend, in that HCA > PCA > 1,1,1,2-TeCA >1,1,1-TCA > 1,1,2,2-TeCA >1,1,2-TCA > 1,1-DCA. Moreover, the k_{SA} values of these chlorinated ethanes linearly correlate with the one-electron reduction potential (E1) and the lowest unoccupied molecular orbital (LUMO) energy of chlorinated ethanes used in the LFERs (Song and Carraway 2005). In contrast, chlorinated ethenes do not follow the proposed trend. As shown in Fig. 3.1 and Table 3.1, the k_{SA} of PCE is lower for TCE for bare Fe^{H2} (RNIP) (Liu et al. 2007; Fagerlund et al. 2012). A similar finding was also reported for ZVI for all the series of chlorinated ethene (i.e., k_{SA} of PCE < TCE < DCEs < VC) (Arnold and Roberts 2000). Based on this finding, Arnold and Roberts (2000) hypothesized that for chlorinated ethene, the transfer of a single electron is not the rate-limiting step but rather the formation of a di-σ-bonded intermediate (Fig. 3.4). This may also explain the findings on NZVI for TCE and PCE.

Noticeably, NZVI reduction is known to be incapable of completely treating 1,2-DCA (Maes et al. 2006; Deng and Hu 2007; Su et al. 2012a). The pseudo-first-order rate constants of 1,2-DCA using NZVI at the concentration of 0.4 g/L and at neutral pH were less than 5×10^{-5}/h (Table 3.1) (Song and Carraway 2005). The poor dechlorination efficacy of 1,2-DCA using NZVI may be due to the relatively high C–Cl bond strength (87.2 kcal/mol) (Cioslowski et al. 1997) compared to the higher chlorinated ethanes. For example, the bond strength of HCA and 1,1,1-TCA was 68.83 and 73.6 kcal/mol, respectively, while the k_{SA} of HCA was four times greater than that of 1,1,1-TCA using Pd/Fe^0 nanoparticles under the same experimental conditions (Lien and Zhang 2005).

Arnold and Roberts (2000) implied that the slow dechlorination rate of 1,2-DCA by ZVI is explainable by the slow formation of a di-σ-bonded intermediate. Recently, sulfidation of NZVI using dithionite was found to degrade more than 90% of 1,2-DCA, but over the course of a year, pseudo-first-order rate constants ranged from 3.8×10^{-3} to 7.8×10^{-3}/day (Garcia et al. 2016); for more details about NZVI sulfidation, see Chap. 9). Even with this novel NZVI modification, the

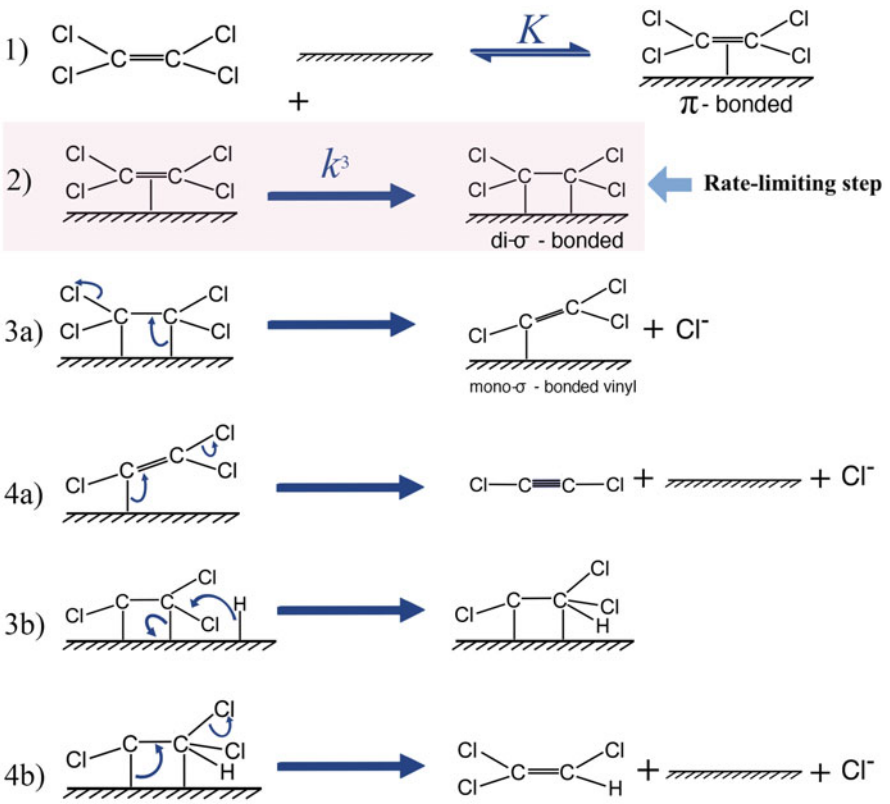

Fig. 3.4 Hypothesized rate-limiting step of the PCE dechlorination by ZVI (i.e., formation of a di-σ-bonded intermediate). After this step, the reaction may proceed via Steps 3a and 4a to give the reductive β-elimination product dichloroacetylene or via Steps 3b and 4b to give the hydrogenolysis product TCE (Arnold and Roberts 2000). (Adapted with permission from Arnold and Roberts (2000). Copyright (2000) American Chemical Society)

reductive dechlorination rate constants are still relatively low and may not be practical for source zone treatment of 1,2-DCA. In contrast, the Fenton process has shown its full potential to degrade 1,2-DCA. The NZVI-induced Fenton's reaction will be discussed more in the latter part of this chapter.

3.1.1.3 Chlorinated and Aromatic Nitro Hydrocarbon

Chlorinated aromatic hydrocarbon, such as chlorophenols, can be detoxified by NZVI to yield a much less hazardous byproduct, such as phenol. Nevertheless, the dechlorination rate constant of pentachlorophenol (PCP) by bare NZVI is relatively low ($K_{obs} = 0.001$/h using smectite-templated Fe^0 containing 13.3 g/L of smectite and 7 mM Fe^0). Thus, to improve the treatability, a Pd catalyst (0.8 mM Pd^0) was added to the nanocomposite, yielding the dechlorinate rate constant of 0.487/h.

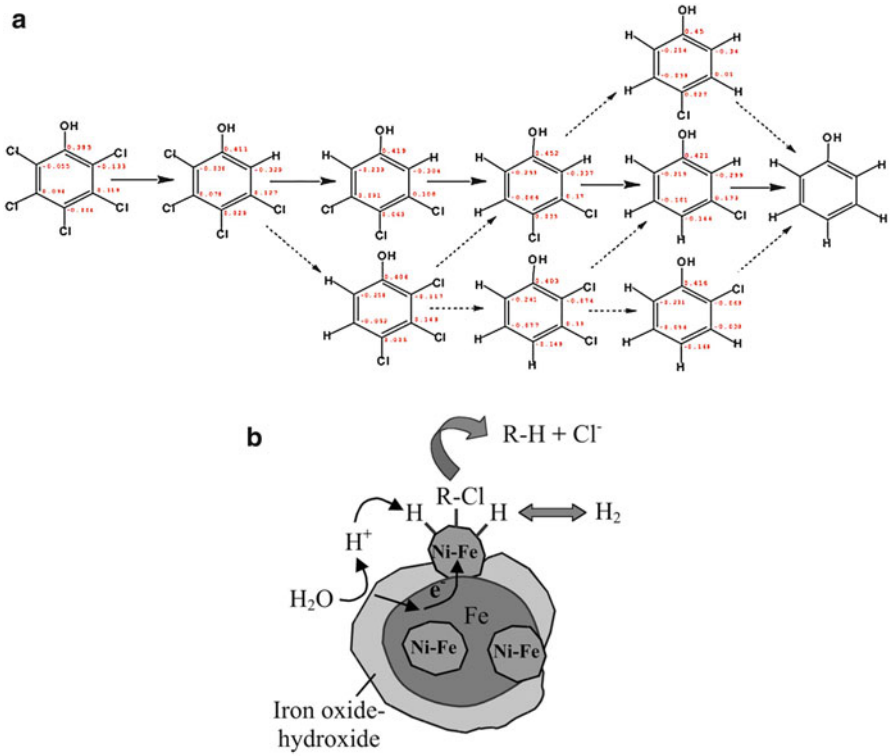

Fig. 3.5 (**a**) Primary dechlorination pathways of chlorinated phenols by smectite-templated Pd^0/Fe^0. Solid arrows refer to the major reaction route, and broken arrows refer to the minor reaction pathway (Jia and Wang 2015) and (**b**) hydrodechlorination driven by Pd^0/Fe^0 nanoparticles (Schrick et al. 2002). (Reprinted with permission from Schrick et al. (2002) and Jia and Wang (2015). Copyright (2015) Elsevier and Copyright (2002) American Chemical Society)

Figure 3.5a illustrates dechlorination pathways of chlorinated phenols by smectite-templated Pd^0/Fe^0 (Jia and Wang 2015).

Hydrodechlorination (Eq. 3.5) is the main dechlorination pathway for such a catalytic NZVI. Protons in the aqueous solution acquire electrons from NZVI, forming hydrogen radical on the Pd surfaces (Fig. 3.5b). In this process, the active H atom formed by Pd^0/Fe^0 attacks the chlorinated phenols via electrophilic H addition to the π system of the benzene ring (formation of H-aromatic complexes) and then removes the chlorine atom by two-electron transfer. Since this process is promoted by electrophilicity of the chlorinated aromatic hydrocarbon, the more chlorinated the phenols, the lower the dechlorination rate with Pd^0/Fe^0 particles because electron-withdrawing groups, such as Cl, that are attached to the aromatic ring reduces the electron density associated with the ring carbons, decreasing the probability of complexation between active H and the corresponding aromatic ring (Jia and Wang 2015). The selectivity of dechlorination of chlorinated phenols is

mainly due to charges and steric hindrance governed by the interaction of substituent Cl atoms and individual aromatic carbon.

Figure 3.5a also shows the calculated charge on each carbon of chlorinated phenols in red. Substituent Cl at the ortho-position is preferentially dechlorinated from the phenol ring due to more negative charges associated with the ortho-position C, which is attributed to the influence of the adjacent OH group. The H in the formed H-aromatic ring complexes is prone to interact with more negatively charged carbon, leading to the scission of the CCl bond (Jia and Wang 2015).

Steric hindrance is another important factor governing the dechlorinate rate of chlorinated phenols. For example, for those chlorinated phenols not containing ortho-Cl, Cl located at the meta-position can be dechlorinated radially due to less steric hindrance. Consequently, as summarized in Table 3.1, the dechlorination rate constants of chlorinated phenols follow the order: PCP < 2,3,4,5-TeCP ~ 2,3,4,6-TeCP ~ 2,3,5,6-TeCP <2,3,4-TCP~2,3,6-TCP ~ 2,4,6-TCP < 3,4,5-TCP ~ 2,4,5-TCP ~ 2,3,5-TCP < 2,6-DCP < 3,5-DCP < 2,3.DCP ~ 2,4-DCP ~ 3,4-DCP < 2,5-DCP < 4-CP ~ 2-CP < 3.CP (Jia and Wang 2015).

Similarly, NZVI and bimetallic NZVI can sequentially dechlorinate chlorobenzenes yielding PeCB, TeCBs, TCBs, and DCBs as byproducts. Unlike chlorophenols, no selectivity of dechlorination product formation was observed for the case of HCB (Zhu et al. 2010). Noticeably, HCB dechlorination is not complete (i.e., no substantial formation of benzene was detected). Interestingly, for HCB dechlorination, Cu appears to be a better catalyst than Pd (Shih et al. 2009; Zhu et al. 2010). Furthermore, nitroaromatic compounds (NACs), such as para-nitrochlorobenzene (p-NCB), are treatable by Ni/Fe^0 nanoparticles. In addition, Ni plays the role of catalyst, decreasing the activation energy of hydrogenolysis of C–Cl bonds, while Fe^0 supplies electrons and reduces H^+ to produce hydrogen gas. Complete transformation (100% removal efficiency) is achieved using Ni/Fe^0 (2.0% Ni) at the concentration of 6 g/L after 300 min. The p-NCB is first adsorbed by NZVI and then quickly reduced to p-chloroaniline (p-CAN) and eventually to aniline (AN) via hydrogenolysis (Xu et al. 2009).

3.1.1.4 Halogenated Bisphenol a (Flame Retardant)

Bimetallic NZVI can completely dechlorinate halogenated bisphenol A, especially at a slightly acidic pH (pH 5–6). Two dehalogenation mechanisms take place simultaneously for different degrees at different pH ranges. Using debromination of tetrabromobisphenol (TBBPA) by Ni/Fe^{H2} nanoparticles as an example, at pH ranging from 3 to 9, sequential dehalogenation via hydrogenolysis takes place as shown in pathway (a) in Fig. 3.6. This hydrogenolysis yields brominated intermediates, such as tri-, di-, and mono-BBPA, as well as a small amount of bisphenol A (BPA; 7.2–7.6%) (Li et al. 2016, 2017). Nevertheless, at a slightly acidic pH (pH 5–6), concerted hydrogenolysis (pathway (b) in Fig. 3.6) is dominant, yielding BPA as a major byproduct (90.7–93.3%) with a small amount of tri-, di, and mono-BBPA (Li et al. 2016, 2017).

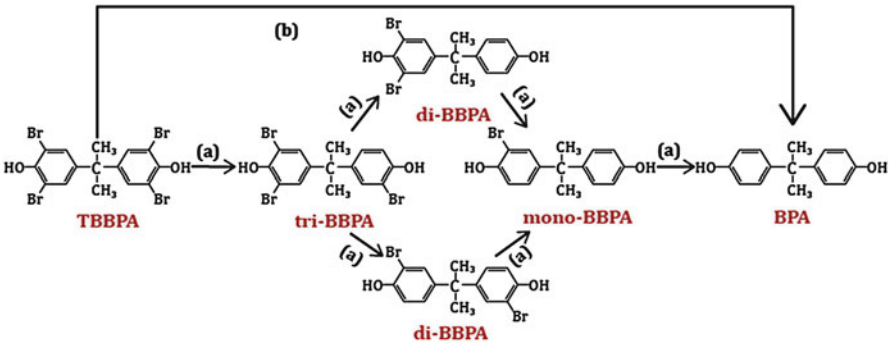

Fig. 3.6 Proposed primary debromination pathways of TBBPA by Ni/NZVI at different initial pHs (a) pH 3.0, 5.0, 6.0, 7.0, and 9.0 and (b) pH 5.0 and 6.0 (Li et al. 2016). (Reprinted with permission from Li et al. (2016). Copyright (2016) Elsevier)

3.1.1.5 Pesticides and Dyes

The NZVI can completely transform complex chlorinated pesticides, such as γ-hexachlorocyclohexane (known as lindane) in 24 h at a NZVI concentration of 0.1–0.39 g/L (Elliott et al. 2009). Figure 3.7 summarizes the degradation pathway of lindane, yielding γ-3,4,5,6-tetrachlorocyclohexene (TeCCH) as a major intermediate with benzene as a byproduct. The dihalo-elimination of vicinal chlorides from carbons 1 and 2 of lindane is supposed to be the first and rate-limiting step. Initially, lindane must adsorb onto the NZVI surface. Then, an electron from Fe^0 is donated to the surface-associated lindane, forming a neutral radical with the release of a chloride ion. Another electron is then transferred from the transient Fe^+ species to the reacting carbon center of the radical, which then undergoes double bond formation and simultaneous release of chloride from the beta carbon, yielding TeCCH as an intermediate. Noticeably, both chlorine atoms (from carbons 1 and 2 of lindane) occupy axial positions on their respective carbon centers and are oriented antiperiplanar, which maximizes their susceptibility toward reduction. After this initial step, the two subsequent dihalo-elimination steps are believed to occur more rapidly, yielding benzene and chloride as major end products (Elliott et al. 2009).

The NZVI can also decolorize dye-contaminated water. Figure 3.8 is an example of the reductive decolorization of methyl orange (MO). It starts with MO adsorption onto the NZVI surface by the formation of the chelate complex of Fe(II) dye. The radicals of H were generated by the NZVI reduction of water or hydrogen ion. Two H radicals were involved in the cleavage of the azo bond with two more electron transfers from NZVI. An electron is transferred from NZVI to the –N=N– bond, causing the breakage of the bond and the combination of a radical of H. In the meantime, another NZVI integrated another two radicals of H to break the N–N bond under the similar process. Eventually, the azo-double bond –N=N– was disconnected from two different amines. The breakage of the azo-double bond makes the visible absorption peaks at 464 nm vanish.

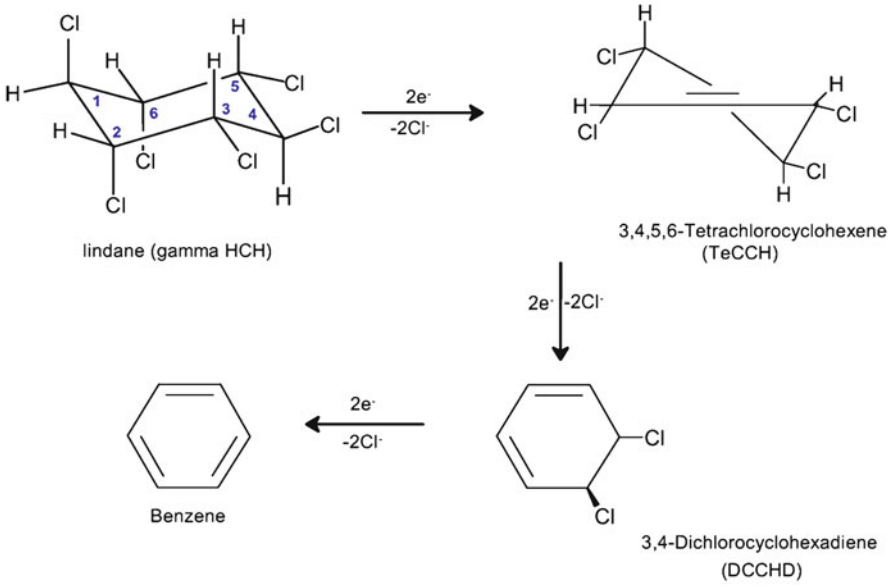

Fig. 3.7 Dihalo-elimination degradation pathway from lindane to benzene (Elliott et al. 2009); with permission from ASCE). (Reprinted with permission from Elliott et al. (2009). Copyright (2016) American Society of Civil Engineers)

3.1.2 Particle Properties Affecting NZVI Reactivity

Table 3.1 summarizes dechlorination rate constants of various contaminants. Noticeably, the rate constants for the same kind of contaminants by different types of NZVI can be substantially different. Although NZVI has two common characteristics, the small size and high specific surface area, NZVI has a vast variety of physicochemical properties, which can enormously affect dechlorination pathways and kinetics. Since the mass of NZVI needed for remediation and thus the cost of the treatment depend on particle reactivity, reactive lifetime, and particle efficiency, all of which are controlled by NZVI physicochemical properties, it is worth elaborating their effects on NZVI performance in this section.

3.1.2.1 Particle Crystallinity and Chemical Composition (Noble Metal)

The previous section discusses the different degradation pathways of various contaminants. Nevertheless, it also notes that different types of bare NZVI, such as Fe^{BH} and Fe^{H2}, have an important contribution to degradation pathways. This is mainly due to the difference in their crystallinity. According to multiple lines of evidence from the transmission electron microscope (TEM), energy-dispersive

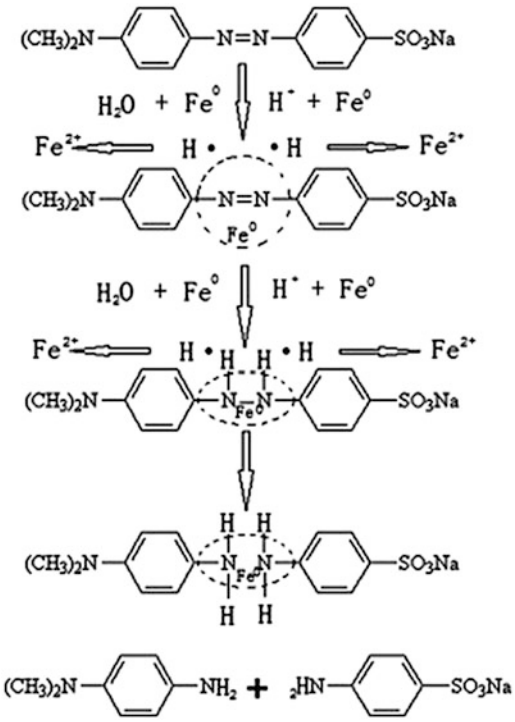

Fig. 3.8 Proposed mechanism for the degradation of MO using Fe^0 nanoparticles (Chen et al. 2011b). (Reprinted with permission from Chen et al. (2011b). Copyright (2011) Elsevier)

spectroscopy (EDS), electron energy-loss spectroscopy (EELS), and X-ray diffraction (XRD) (Liu et al. 2005a, b; Nurmi et al. 2005; see also Chap. 2), the morphology of Fe^{H2} appears to be a crystallographic angular structure rather than a round, amorphous shape-like Fe^{BH}. While no significant oxide shell was observed for Fe^{BH} (Liu et al. 2005b), the iron oxide phases, such as magnetite and maghemite, were observed as the stabilized shell of Fe^{H2} (Liu et al. 2005b; Nurmi et al. 2005; Baer et al. 2007; Reinsch et al. 2010). This crystallinity and iron oxide shell critically govern particle reactivity, particle lifetime, and particle efficiency (Liu et al. 2005b; Nurmi et al. 2005).

As shown in Table 3.1, using TCE as an example, the k_{SA} value using Fe^{H2} (0.35 g/L) is 4×10^{-4} L/(h·m^2), while the k_{SA} value using Fe^{BH} is 2×10^{-3} L/(h·m^2) at the same experimental condition. This is a fivefold difference in k_{SA} values (Liu et al. 2005b). The similar trend is also reported for the dechlorination of tetrachloromethane using Fe^{BH} and Fe^{H2} (Nurmi et al. 2005). This is because amorphous Fe^{BH} can utilize H_2 produced from the H^+ reduction for TCE dechlorination through a catalytic hydrodechlorination pathway (Liu et al. 2005a). This increases efficiency of electron utilization for Fe^{BH} because electrons used to produce H_2 can then be used to degrade TCE. This feature is not available in crystalline Fe^{H2}, making its TCE dichlorination rely on β elimination and hydrogenolysis only. Thus, for Fe^{H2}, the electron used to produce H_2 is considered unproductive with respect to dechlorination. Nevertheless, due to their amorphous Fe^0 and the absence of an iron oxide shell, at pH 7, a relatively large fraction of Fe^0

in Fe^{BH} interacted with H^+ and was used to produce H_2, implying that Fe^{BH} has a poor selectivity of electron utilization for dechlorination (Liu et al. 2005a).

In the same conditions, a relatively small fraction of Fe^{H2} was used to produce H_2, implying that Fe^{H2} has a good selectivity of electron utilization for dechlorination (Liu et al. 2005b; Liu and Lowry 2006).

In addition to particle crystallinity, different chemical compositions of Fe^{BH} and Fe^{H2} also affect the electron utilization efficiency. Unlike the case of Fe^{H2}, the formation of iron oxide film around Fe^{BH} was not observed due to the presence of boron in Fe^{BH} particles that facilitated the dissolution of the particles and thus regenerated the reactive sites for TCE dechlorination. Consequently, almost all of the Fe^0 in Fe^{BH} was available for dechlorination (i.e., high particle efficiency ~92%; (Liu et al. 2005a, b)). On the other hand, the iron oxide shell grew as RNIP (commercially available Fe^{H2}) was oxidized, making some fraction of Fe^0 in RNIP unavailable for dechlorination (Liu et al. 2005b). Consequently, particle efficiency went down (only around 52%). However, the disadvantage of Fe^{BH} particles is their relatively short lifetime in comparison to Fe^{H2}. For in situ remediation, a long reactive lifetime is preferable for cost-effective treatment of contaminant plumes and to ensure that NZVI particles do not "burn out" prior to reaching contaminated areas (Liu et al. 2005b).

In addition to the effect of boron in Fe^{BH} on particle dissolution, another example of the influence of chemical composition on NZVI reactivity is the bimetallic NZVI (i.e., NZVI doped with Pd, Pt, Cu, and Ni) to enhance particle reactivity through catalytic pathways (Zhang et al. 1998; Schrick et al. 2002; Zhang 2003). The structure of bimetallic NZVI particles is a reductive Fe^0 core with the shell of inert noble metals (Fig. 3.5b as an example). Because of the presence of noble metals, bimetallic particles can utilize H_2 for hydrodechlorination (Zhang 2003). As shown in Table 3.1, using chlorinated ethane and ethene as examples, k_{SA} or k_{obs} using bimetallic NZVI is around 10–50 times greater than bare NZVI. However, a significant problem with bimetallic NZVI is the observed decrease in reactivity over time due to the deactivation if the thick oxide layer can form and cover the noble metals (Zhu et al. 2006). This deactivation issue is an important obstacle for long-term remediation using bimetallic NZVI.

3.1.2.2 Effect of Polymeric Surface Modification

Polymeric surface modification, as a means to increase NZVI mobility in the subsurface and affinity for specific subsurface contaminants (Chaps. 5 and 6), is essential for in situ remediation using NZVI. However, polymeric surface modification may either enhance or decline NZVI reactivity toward organic contaminants. Since the dechlorination reactions are heterogeneous (the contaminant must contact the particle surface to be degraded), NZVI synthesis in the presence of polymers or polyelectrolytes, such as carboxymethyl cellulose (CMC), guar gum, and polyvinylpyrrolidone (PVP), in a "one pot" manner appears to enhance NZVI reactivity. This surface modification approach yields smaller particles in comparison

to the physisorption of polymers or polyelectrolytes onto pre-synthesized NZVI. Conceptually, the Fe^{2+} or $Fe3^{+}$ ions from $FeSO_4$ or $FeCl_3$ may be complexed with polyelectrolytes prior to reductive precipitation using $NaBH_4$. The complexed Fe^{2+} or Fe^{3+} ions behave as nucleation seeding points of NZVI. Consequently, we obtained polymer-modified NZVI with a smaller size that was resistant to aggregation and, thus, more reactive than larger, non-stabilized NZVI. This results in the observed increases in TCE reactivity with polymer-modified Fe-Pd bimetallic nanoparticles at low polyelectrolyte concentrations compared with bare Fe-Pd bimetallic nanoparticles (He and Zhao 2008; Sakulchaicharoen et al. 2010) (Table 3.1).

Nevertheless, the opposite is true for polymeric surface modification of pre-synthesized NZVI, in that polymeric surface modification can decrease the NZVI reactivity via reactive site blocking and mass-transfer resistance. As seen in Fig. 3.9a, the polymeric modified NZVI is covered with a layer of adsorbed macromolecules. According to the Scheutjens and Fleer conceptual model for homopolymer sorption (Scheutjens and Fleer 1979, 1980), charged homopolymers are normally adsorbed onto the surface in the train-loop-tail configuration.

Trains are segments of polymer directly attached to the particle surface, which can block NZVI reactive sites, whereas loops and tails form an extended polyelectrolyte brush away from the surface, which can retard the diffusion of chlorinated volatile organic compounds (CVOCs) from the bulk aqueous solution to the NZVI surface. Similarly, for random copolymer, block copolymer, or grafted polymer, trains or anchoring blocks may block electron transfer sites, while a polymer brush may limit the mass transfer or chlorinated organics to the reactive NZVI surface. Several recent studies support this hypothesis. As summarized in Table 3.1, Phenrat et al. (2009a) revealed that, when the surfaces of pre-synthesized NZVIs were modified by the physisorption of polyelectrolytes, the TCE dechlorination rate constant decreased nonlinearly with the increasing adsorbed mass of the polyelectrolytes, with a maximum 24-fold decrease in reactivity. This is due to reactive site blocking and a decrease in the aqueous TCE concentration at the surfaces of the NZVIs due to the partitioning of TCE to the adsorbed polyelectrolytes. A similar finding was also reported by Wang and Zhou (2010) using solvent-responsive, polymer-coated NZVIs to degrade TCE (Wang and Zhou 2010). Noticeably, for the case of "one pot" polymer-modified NZVI, we believe that polymer still blocks the NZVI reactive site and still resists CVOC mass transfer to the NZVI surface, but the two adverse effects are outweighed by the positive effects from the smaller size of NZVI.

Nevertheless, polymeric surface modification makes the NZVI less sensitive to environmental factors in comparison to bare NZVI. As summarized in the next section, non-reducible ionic species, such as Cl^{-}, SO_4^{2-}, HCO_3^{-}, and HPO_4^{2-}, decreased the TCE dechlorination rate constant by bare NZVI up to a factor of seven compared with deionized (DI) water at pH 8.9 (Liu et al. 2007). On the other hand, polymeric surface modification reduces the interaction of NZVIs with nontarget groundwater solutes (organic and ionic species). A possible explanation is the effect of the Donnan potential in the polyelectrolyte layer on ionic solute distributions. The Donnan potential (Fig. 3.9b, c) can decrease the concentration of cationic solutes at

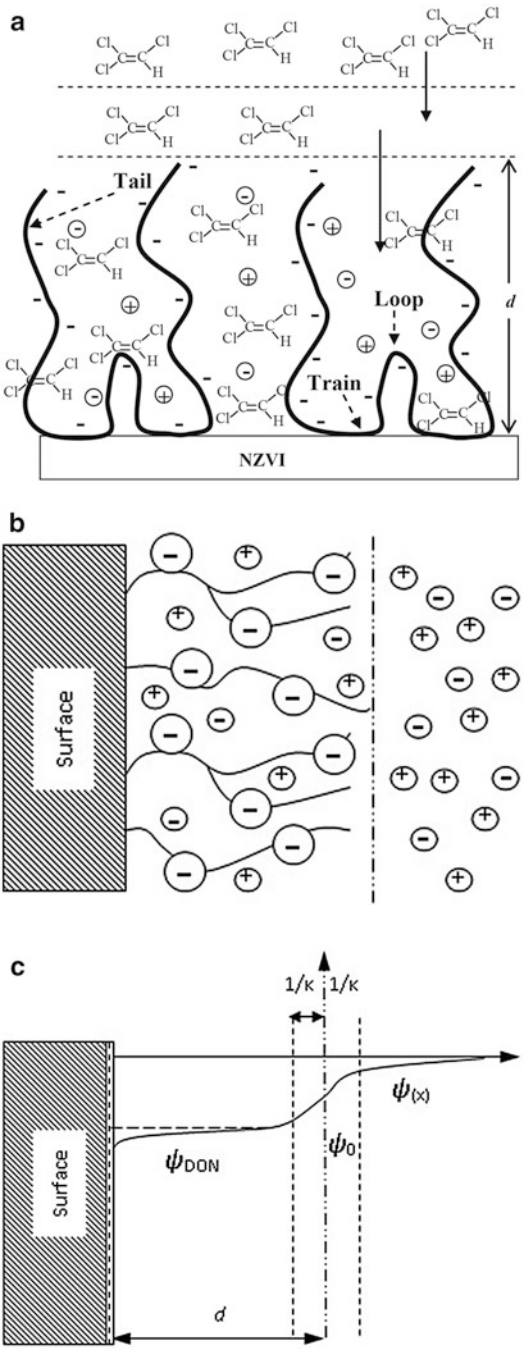

Fig. 3.9 Schematic illustrating site blocking due to adsorbed trains and formation of an extended brush layer (**a**) of loops and tails (Phenrat et al. 2009b) and (**b**, **c**) effect of the Donnan potential in the polyelectrolyte layer on ionic solute distributions (Phenrat et al. 2015). (Reprinted with permission from Phenrat et al. (2009b, 2015). Copyright (2009) American Chemical Society and Copyright (2015) Springer Nature)

the surfaces of NZVIs and possibly reduce their blocking effect compared with that for bare NZVIs. A recent study reported that for the first TCE spike, TCE dechlorination rates using polyaspartate (PAP)-modified NZVIs in the actual groundwater samples were 70–85% of the TCE dechlorination rate using PAP-modified NZVIs in DI water (Phenrat et al. 2015), while the TCE dechlorination rates using bare NZVI in the same groundwater samples for the first TCE spike were around ~22% of the TCE dechlorination rate using bare NZVIs in DI water.

Furthermore, over an intermediate period (30 days), in the presence of groundwater solutes, polyelectrolytes, such as PAP, were desorbed from NZVI and thus restored the reactivity of bare NZVIs with TCE. Evidently, the TCE dechlorination rates using PAP-modified NZVIs in the second and third TCE dechlorination cycles (intermediate-term effect) increased substantially (~100% and 200%, respectively, from the rate of the first spike). The desorption of PAP from the surface of NZVIs over time due to salt-induced desorption is hypothesized to restore NZVI reactivity with TCE (Phenrat et al. 2015). This suggests that the modification of the NZVI surface with small charged macromolecules, such as PAP, helps to deliver NZVIs to the subsurface and restores NZVI reactivity over time due to a gradual PAP desorption in groundwater.

3.1.2.3 Sorptive Support

Another means to increase NZVI mobility in the subsurface and the affinity for specific subsurface contaminants is using NZVI supports, such as submicron- or micron-sized porous silica (Zheng et al. 2008) or activated carbon (Mackenzie et al. 2012). These particles serve as carriers for NZVI transport because incorporation of NZVI into porous particles decreases the extent of magnetic attraction among NZVI particles, leading to less agglomeration and increasing their subsurface mobility. Furthermore, these supports are typically sorptive for organic contaminants; the NZVI composite materials behave as sorptive and reactive remediation agents. Figure 3.10 illustrates the dual-phase TCE removal mechanism by Fe^{BH} entrapped in porous ethyl-functionalized silica (Fe(B)/ethyl-silica system). Noticeably, an immediate sharp decrease of the aqueous TCE concentration to 45% of its original value was observed due to TCE sorption onto the functionalized silica followed by a much slower reaction rate, presumably due to dichlorination. Figure 3.10 also shows the byproduct formation, which supports the sorptive and reactive removal of TCE by the Fe(B)/ethyl-silica system.

Similar behavior is also observed by carbo-iron colloid (CIC), which is Fe^{H2} encapsulated in activated carbon. The sorptive and reactive TCE removal mechanism contributes to the higher reactivity and more NZVI utilization efficiency in comparison to bare NZVI without support. Mackenzie et al. (2012) showed that, for bare Fe^{H2}, dichlorination rate constants (k_{obs}) decreases with the decrease of the NZVI concentration, while the rate constants (k_{obs}) for CIC are insensitive to the CIC concentration in the suspension. This is because almost all TCE is adsorbed to the activated carbon of CIC, and since the dechlorination takes place at the surface, the

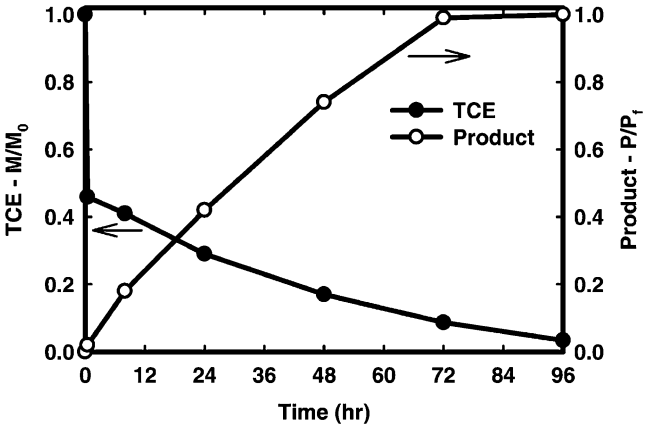

Fig. 3.10 TCE removal from solution and gas product evolution rates for Fe(B)/ethyl−silica, where M/M_0 is the fraction of the original TCE remaining, and P/P_f is the ratio of the gas product peak to the gas product peak at the end of 96 h (Zheng et al. 2008). (Reprinted with permission from Zheng et al. (2008). Copyright (2008) American Chemical Society)

reaction rate is determined by the Fe^0 content of the carbo-iron and not by the total Fe^0 concentration in the suspension (Mackenzie et al. 2012).

3.1.2.4 Aging Effect

Aging or longevity is the change of NZVI during immersion in water mainly by reacting with oxygen, water, target contaminants, or naturally occurring subsurface constituents. It can seriously affect both NZVI morphology and reactivity. Because in situ remediation is a moderate- to long-term operation, NZVI aging should be accounted for in determining the required amount of NZVI for contaminant transformation.

Typically, NZVI has a core (Fe^0) and shell (iron oxide, such as magnetite and maghemite) structure. Aging is a dynamic and complex process conceptually consisting of three processes including (1) breakdown of the existing oxide shell by hydration and auto reduction, (2) oxidation of the freshly exposed underlying Fe^0 coupled with reduction of reactive solutes, such as oxygen or target contaminants, and (3) subsequent cementation by formation of authigenic mixed-valent Fe(II)-Fe(III) phases (Sarathy et al. 2008). The aging phenomenon is substantially affected by the type of NZVI (Fig. 3.11) (Kim et al. 2012).

For Fe^{BH}, the aging model is described by the outward diffusion of the Fe^0 core toward the shell. This results in the formation of hollowed-out iron oxide shells, which are further transformed into sheet- and needle-shaped materials (Liu et al. 2015). Various secondary iron oxide mineral phases were formed at different aging times. For example, at 5 days, the main iron oxide shell is magnetite (Fe_3O_4) and maghemite (γ-Fe_2O_3), accompanied by lepidocrocite (γ-FeOOH). For 10-day

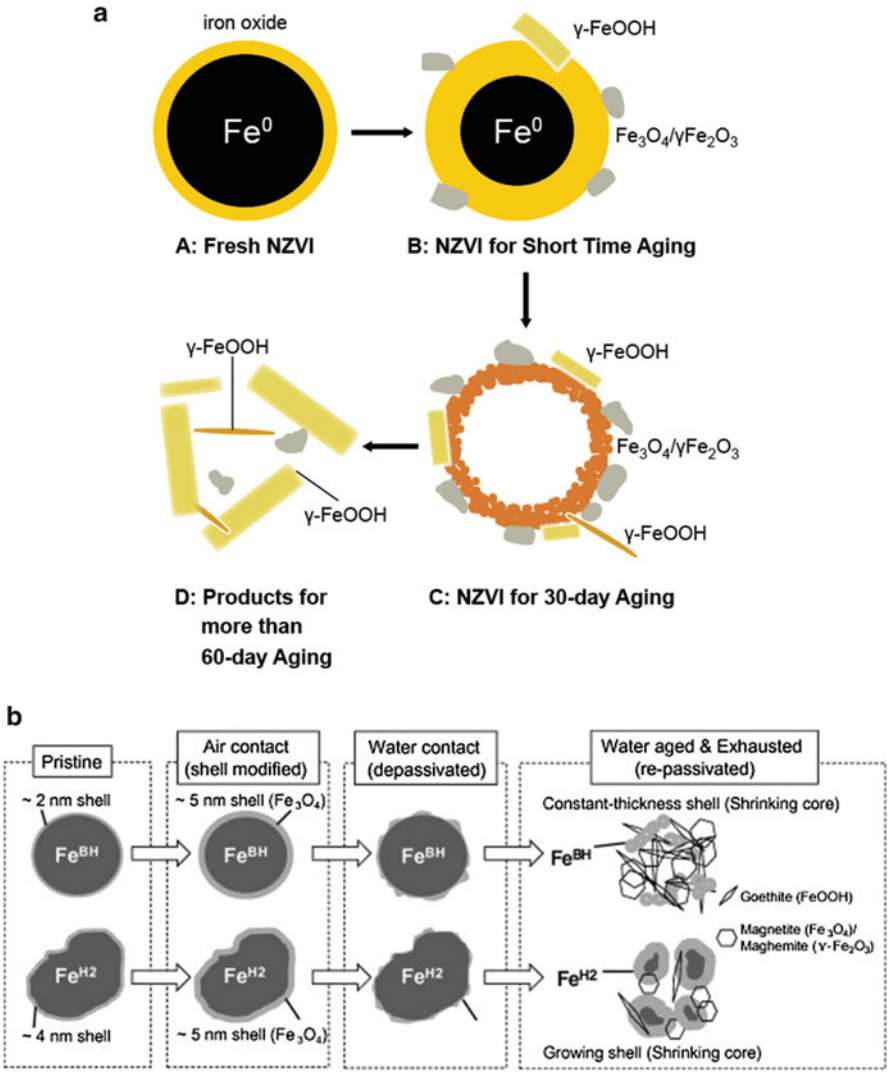

Fig. 3.11 Schematic description of the aging procedures of Fe^{BH} and Fe^{H2} nanoparticles (**a**) from Kim et al. (2012) and (**b**) from Liu et al. (2015). (Reprinted with permission from Kim et al. (2012) and Liu et al. (2015). Copyright (2012 and 2015) Elsevier)

aging, the ferrihydrite and lepidocrocite were dominant. When aged up to 90 days, the products are mainly γ-FeOOH mixed with small amounts of Fe_3O_4 and γ-Fe_2O_3, as also evident by the formation of the sheet- and needle-shaped materials, the typical morphology of lepidocrocite (Liu et al. 2015). Due to their high reactivity and the outward diffusion of Fe^0 core, Fe^{BH} aging can substantially

consume Fe^0, resulting in a significant decrease of Fe^{BH} reactivity over time (Wang et al. 2010). A similar decrease in reactivity was also reported in Pd/Fe^{BH} particles in which aging causes both catalyst deactivation (i.e., Pd was completely buried underneath an extensive iron oxide matrix) and Fe^0 depletion (Yan et al. 2010). The CMC-modified Fe^{BH} was affected by aging in a similar manner. Nevertheless, the coating of CMC could slow the aging rate of Fe^{BH} as indicated by the slower drop in Fe^0 intensity in the XRD pattern (Dong et al. 2016). Moreover, CMC was found to influence the transformation of Fe^0 and the formation of iron oxide because greater CMC loading in the suspension results in more the lepidocrocite formation as a corrosion product of CMC-modified Fe^{BH}.

Unlike Fe^{BH}, aging of Fe^{H2} follows a growing shell and shrinking core model with no outward diffusion of Fe^0 core. The periods of increased, declined, and stabilized reactivity were observed during the aging of Fe^{H2}. Liu and Lowry (2006) studied reactivity changes with aging of Fe^{H2} using TCE as a reactivity probe. They observed a significant initial decrease (for the first 10 days) in TCE reaction rate constants ($k_{obs,TCE}$) for Fe^{H2} ($Fe^0 = 48\%$) decreased from 6.2×10^{-3} L/(h·m^2) to 1.0×10^{-3} L/(h·m^2) after 10 days (Liu and Lowry 2006). They interpreted the initial decrease as the healing of defects in the oxide film formed when the particles were removed from the concentrated suspension and dried. This is followed by a constant or slightly increasing rate constant during which the Fe^0 content of the particles decreased by ~40%. Thus, they concluded that the TCE reaction is zero-order with respect to the Fe^0 content of Fe^{H2}.

Eventually, reactivity with TCE ceased after 170 days when the Fe^0 content reached ~4.6%. A similar trend was observed by Sarathy et al. (2008) who used tetrachloromethane as a reactivity probe. They reported the increase of dechlorination rate constants of tetrachloromethane at the initial state (1–2-day exposure of dried Fe^{H2} to DO/DI water) followed by a gradual decrease over 1–6 months of aging (depending on the drying procedure of the Fe^{H2}). The initial increase in reactivity was explained by depassivation of the particles soon after the first immersion of dried Fe^{H2} in water. The depassivation involves breakdown of the iron oxide shell, thereby exposing the underlying Fe^0 core to the target contaminant. The gradual decrease in dechlorination rate constants after 1–2 days suggests the repassivation due to growth of a new oxide shell or transformation of the oxide shell, which gradually stabilizes the electron transfer from the Fe^0 core.

3.1.3 Environmental Factors Affecting NZVI Reactivity

Table 3.1 summarizes the batch experiments for reductive treatment of various kinds of organic contaminants using various kinds of NZVI. Most of the studies were conducted in a batch system in DI water at a pH of 8–9, representing an $Fe(OH)_2/H_2O$ or Fe_3O_4/H_2O equilibrium. However, NZVI particles are applied in a subsurface environment, which is far more complex than DI water. The presence of dissolved inorganic and organic species, dense nonaqueous phase liquid

(DNAPL), and aquifer materials in the subsurface can physically and chemically affect the performance of NZVI particles. For this reason, this section reviews the effects of these environmental factors on NZVI performance.

3.1.3.1 pH

Groundwater pH typically varies from 6 to 8. The application of NZVI for in situ remediation is normally at only 0.2–0.5 wt %. Thus, because of the high buffer capacity of most soil, the groundwater pH will not change much due to the injection and emplacement of NZVI. Consequently, groundwater pH can substantially affect the electron utilization and lifetime of NZVI (Liu and Lowry 2006). As shown in Eq. (3.3), H^+ can consume Fe^0 to produce H_2. This is controlled by pH and competes with electron utilization for dechlorination (Eq. 3.2). Therefore, at low pH, Fe^0 tends to be utilized for H_2 production rather than dechlorination. For Fe^{H2}, the H_2 evolution rate constant increased by 27-fold (from 0.008 to 0.22 day^{-1}) due to decreasing pH from 8.9 to 6.5 (Liu and Lowry 2006). However, the TCE dechlorination rate constants were only two times higher (Liu and Lowry 2006). The increase of the TCE dichlorination rate constant is 1.44/h with respect to a one unit decrease of pH.

A similar trend was also observed for Fe^{BH} for dichlorination of trichloromethane (Song and Carraway 2006) and 1,1,2,2-tetrachloroethane (Song and Carraway 2005) of which the dichlorination rate constants increase by 0.33 and 0.24/h per one unit decrease of pH, respectively. Rapid H_2 evolution and Fe^0 consumption yield a relatively short lifetime of NZVI. At a pH of 6.5, the reactive lifetime of Fe^{H2} was only around 2 weeks (Liu and Lowry 2006). For this reason, both particle lifetime and efficiency decline due to the decrease of pH. The adverse effect of low pH becomes more severe when NZVI particles are applied to treat groundwater plumes in comparison to the source zone treatment because, in plumes, a low concentration of target contaminant is available for reaction with NZVI, and most Fe^0 will be used for H_2 production. In conclusion, the application of NZVI particles to treat contaminant plumes in aquifers with low pH (~6.5) is not favorable, and additional NZVI injections are expected every few weeks, making it economically unfeasible.

3.1.3.2 Anionic and Cationic Species

Due to geochemical cycles (dissolution and precipitation) of minerals in the subsurface, groundwater normally consists of various anionic species, such as NOO_3^-, Cl^-, SO_4^{2-}, HCO_3^-, and HPO_4^{-2}. Groundwater chemistry can affect NZVI corrosion rate, dechlorination rate, H_2 production, dissolution, and formation of an iron oxide shell. At low concentration (0.2–1 mM), reducible solutes, such as NO_3^-, did not significantly affect the TCE dechlorination rate. However, at high concentration (~5 mM), NO_3^- deactivated Fe^{H2} reactivity toward TCE after 3 days, even though Fe^0 remained in Fe^{H2} (Liu et al. 2007). Similarly, NO_3^-

(7.7 mM) was reported to inhibit dichlorination of hexachlorobenzene using Fe^{BH} (Su et al. 2012b).

Presumably, two possible hypotheses are that, at this high NO_3^- concentration, nitrite may be built up to block reactivity, or nitrate may promote the formation of a passivating and insoluble Fe(III) oxide layer, like maghemite or hematite (Schlicker et al. 2000). However, neither maghemite, hematite, nor goethite was observed using EXAFS (Reinsch et al. 2010), suggesting that the passivating layer may be some other phases or at a too low concentration to be detected using EXAFS. Nevertheless, the passivation by nitrate must happen very rapidly because the Fe^{H2} passivated by NO_3^- contained Fe^0, schwertmannite, and magnetite at the same ratio as fresh Fe^{H2} as if no Fe^0 oxidation took place (Reinsch et al. 2010).

In contrast, non-reducible anions, such as Cl^-, SO_4^{2-}, HCO_3^-, and HPO_4^{-2}, decreased the TCE dechlorination rate up to a factor of seven in comparison to DI water, and the order of their effect follows their affinity of anion complexation to hydrous ferric oxide (i.e., $Cl^- < SO_4^{2-} < HCO_3^- < HPO_4^{2-}$) at pH 8.9 (Liu et al. 2007). This implies that the inhibitory effect of these solutes on TCE degradation may be caused by reactive site blocking due to the formation of Fe-anion complexes on the Fe^{H2} surface. On the other hand, as for dichlorination of HCB using Fe^{BH}, HCO_3^- did not affect the dichlorination rate, while Cl^- and SO_4^{2-} slightly enhanced HCB dechlorination rate constants due to their corrosion promotion (Su et al. 2012b).

Similar to the case of anionic species, cationic species, such as Na^+, Mg^{2+}, Fe^{2+}, Cu^{2+}, Ni^{2+}, Cd^{2+}, and Zn^{2+}, might be released to the groundwater due to geochemical cycles. Furthermore, these pollutants might be found at high concentrations in DNAPL-contaminated areas as co-contaminants. The NZVI has been demonstrated to be effective for the immobilization of various metals (Ponder et al. 2000; Zhang 2003; Dries et al. 2005; Kanel et al. 2005) through reduction (Eq. 3.8), co-precipitation, and surface complexation (Eqs. 3.9 and 3.10) depending on the relative standard potential E^0 between NZVI and metals (Li and Zhang 2007; see Chap. 4).

$$Me^{a+} + be^- \rightarrow Me^{a-b} \tag{3.8}$$

$$\equiv S - OH + Me^{2+} \leftrightarrow \equiv S - OMe^+ + H^+ \tag{3.9}$$

$$2 \equiv S - OH + Me^{2+} \leftrightarrow (\equiv S - O)_2 Me + 2H^+ \tag{3.10}$$

For metal ions such as Zn^{2+} and Cd^{2+}, of which E^0 is very close to or more negative than that of Fe^0, the main removal mechanism is sorption and surface complexation (Li and Zhang 2007). For metal ions such as Ni^{2+} and Pb^{2+}, of which E^0 is slightly more positive than that of Fe^0, the removal mechanism is the combination of reduction and sorption (Li and Zhang 2007). For metal ions such as Cu^{2+}, Ag^+, and Hg^{2+}, of which E^0 is greatly more positive than that of Fe^0, the major removal mechanism is reduction (Li and Zhang 2007). As shown in Eq. (3.8), the reduction of metals consumes electrons (i.e., a competing reaction to dichlorination of chlorinated organics; Eq. 3.2). In addition, the reduction of

metals is normally followed by the precipitation of reduced metals on the surface of NZVI. This co-precipitation reaction with surface complexation (Eqs. 3.9, 3.10, and 3.11) can block reactive sites or promote the formation of Fe(III)-metal oxide, a passivating layer, at anodic sites. This decreases NZVI reactivity for dechlorination. For this reason, in general, the presence of metals as co-contaminants adversely affects the dechlorination rate. For example, in the presence of Zn, TCE degradation using ZVI was 2–4 times slower (Dries et al. 2005). Similarly, in the presence of Cr(VI) at a concentration higher than 5 mg/L, the TCE dechlorination rate decreases by a factor of 3–13 (Dries et al. 2005).

Similarly, Fe(II) inhibited the HCB degradation reaction due to passivation layers formed, while Na^+ and Mg^{2+} did not substantially affect the dichlorination (Su et al. 2012b). However, the presence of noble metals including Cu^{2+}, Ni^{2+}, Pd^{2+}, and Pt^{2+} appeared to enhance the dichlorination rate through the catalytic pathway. The presence of Ni (5–100 mg/L) enhanced the TCE dechlorination due to the catalytic hydrodechlorination by bimetallic Fe^0/Ni^0 from the precipitation of Ni^0 on the surface of ZVI (Dries et al. 2005). Similarly, the presence of Cu^{2+} enhanced dichlorination of HCB (Su et al. 2012b). Furthermore, metal ions including Co^{2+}, Cu^{2+}, and Ni^{2+} enhanced the dechlorination of 4-chlorobiphenyl (4-ClBP) by NZVI. The dechlorination percentages of 4-ClBP in the presence of 0.1 mmol/L of Co^{2+}, Cu^{2+}, and Ni^{2+} were 66.1%, 66.0%, and 64.6% in 48 h, and then increased to 67.9%, 71.3%, and 73.5%, after 96 h, respectively (Wang et al. 2011).

3.1.3.3 Natural Organic Matters in Groundwater and Soil

Groundwater naturally contains a significant amount of natural organic matter (NOM) originated from decomposition of animal and plant bodies (Schwarzenbach et al. 2003b). The NOM is a natural charged macromolecule, carrying a net negative charge at a natural pH due to the dissociation of carboxylic groups (Schwarzenbach et al. 2003a). Furthermore, NOM consists of humic and fulvic acids. By operational definition, humic acid is the fraction of NOM that precipitates at pH 2 or lower, while the fulvic acid fraction stays soluble under all pH conditions (Schwarzenbach et al. 2003a). The NOM was found to adsorb various kinds of colloids and nanoparticles (Ramos-Tejada et al. 2003; Hyung et al. 2007). Similarly, carboxylic groups of NOM can specifically adsorb onto the iron oxide surface of Fe^{H2} (Fig. 3.12a). The NOM is an anionic polyelectrolyte, which tends to adsorb onto the substrate in a train-loop-tail configuration (Fleer et al. 1998) similar to the polyelectrolyte discussed above.

There are two different hypotheses of the effects of NOM on ZVI performance. First, NOM can enhance electron transfer and thus ZVI reactivity for pollutant degradation through electron shuttle effects (Tratnyek et al. 2001). Second, adsorbed NOM decreases ZVI reactivity due to reactive site blocking (Tratnyek et al. 2001; Cho and Park 2006; Doong and Lai 2006). Moreover, consisting of the quinone group with standard potential E^0 of 0.23 V, NOM is hypothesized to transfer electrons from ZVI for the dechlorination of chlorinated ethene (Tratnyek et al. 2001). The enhanced

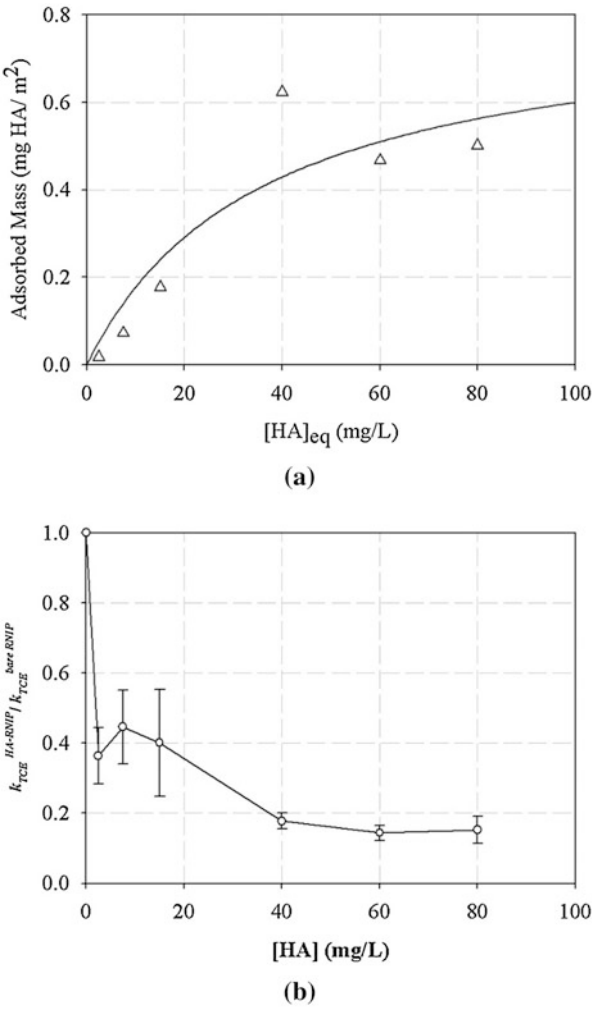

Fig. 3.12 (**a**) Adsorption isotherm of HA on RNIP at pH 8.5; the line illustrates the best fit using the Langmuir isotherm. (RNIP is NZVI formed by reduction using H_2). (b) The relationship between standardized TCE dechlorination rate constants using RNIP and HA concentrations in the aqueous phase

dechlorination due to the presence of humic acid in the ZVI system was observed for PCE dechlorination but not TCE (Cho and Park 2006). In contrast, Tratnyek et al. (2001) reported that TCE degradation kinetics decreased by 21% and 39% in the presence of 20 and 40 mg/L, respectively, of Suwannee River organic matter, presumably due to reactive site blocking.

Figure 3.12b supports and extends the second hypothesis regarding the effect of NOM on TCE dechlorination using NZVI. In the presence of different humic acid concentrations, the TCE dechlorination rates by bare RNIP decreased nonlinearly and exhibited two regions. The TCE dechlorination pathways were not affected, and β elimination remained the dominant dechlorination pathway, yielding acetylene as the reaction intermediate and ethane and ethene as products. Consistent with the

Scheutjens-Fleer theory for homopolymer sorption (Fleer et al. 1998), the nonlinear relationship between the dechlorination rate and the surface excess of adsorbed humic acids suggests that adsorbed humic acids decrease reactivity primarily by blocking reactive surface sites at low surface excess where they adsorb relatively flat onto the Fe^{H2} surface and by site blocking and decreasing TCE availability at high surface excess where humic acids form an extended layer around the particles. This finding is confirmed by a recent study revealing that the presence of Suwannee River humic acids (SRHA) (10 mg/L) decreased TCE (20 mg/L) dechlorination by Fe^{H2} around 23% but did not affect the H_2 production (Chen et al. 2011a). Nevertheless, the mix effect of NOM on NZVI reactivity was also reported. A recent study reported that the presence of humic acid inhibited the reduction of 4-ClBP in the first 4 h, but then significantly accelerated dechlorination by reaching 86.3% in 48 h (Wang et al. 2011).

In addition to the dissolved NOM, the NOM that is adsorbed onto soil or aquifer material can substantially decline dechlorination efficiency. This is an issue of mass transfer of CVOCs from soil to groundwater. The CVOC-sorbed soil may behave as a long-term secondary source, gradually leaching dissolved CVOCs to contaminate the groundwater downgradient. Slow desorption of CVOCs from the soil can result in retardation of reductive detoxification using NZVI. Using TCE as an example, TCE has an arithmetic mean organic carbon partitioning coefficient (k_{oc}) of 86 (ranging from 18.5 to 150). The soil-water partitioning coefficient (k_d) is the k_{oc} x fraction of organic carbon in soil (f_{oc}). This partitioning coefficient can be used to calculate the retardation factor (R) as shown in Eq. 3.11. Subsequently, we can estimate the decrease in TCE dechlorination rate by NZVI in the soil-water system ($k_{TCE\text{-}aq\text{-}Soil}$) with R using Eq. 3.12 in comparison to the TCE dechlorination rate constant using NZVI in water (no sorption onto soil; $k_{TCE\text{-}aq}$):

$$R = 1 + \frac{k_d{}^* \rho_b}{n} \tag{3.11}$$

$$k_{TCE\text{-}aq\text{-}Soil} = \frac{k_{TCE\text{-}aq}}{R} \tag{3.12}$$

where ρ_b and n are the bulk density of soil and porosity, respectively. Under equilibrium with the partitioning coefficient (k_d) of 1.46 L/kg, R is calculated as 7.28 using Eq. 3.11. Thus, the TCE sorption into soil can decrease the TCE dechlorination rate constant in the soil-water system by 7.28 times in comparison to the system with groundwater alone. This is problematic because, instead of using its reducing power to destroy contaminants, the NZVI reacts with the water to form H_2, which increases the amount of NZVI required for remediation (Liu et al. 2007; Berge and Ramsburg 2010). This is a mass-transfer limitation problem that cannot be solved by modifying NZVI to have greater reactivity, such as by doping with catalysts. Instead, a possible solution is to use NZVI with thermal-enhanced CVOC dissolution or desorption, which will speed up the reaction rate and improve the electron utilization efficiency of the remediation (see Chap. 11).

3.1.3.4 TCE Concentration and the Presence of DNAPL

The NZVI particles are proposed for the remediation of both the DNAPL source zone and groundwater plumes. Therefore, NZVI is subjected to a wide range of CVOC concentration, from low concentration in contaminant plumes to near saturation or even DNAPL in the source zone. The different CVOC concentrations in different zones influence electron utilization, particle efficiency, and the reactive lifetime of NZVI. A recent study (Liu et al. 2007) revealed that changing TCE concentrations from low to medium range (0.03–0.46 mM) insignificantly affected the TCE dechlorination rate using Fe^{H2} at pH 7. However, at higher concentrations (1.3 mM) to TCE water saturation (8.4 mM), the TCE dechlorination rate by Fe^{H2} decreased by a factor of two, presumably due to reactive site blocking by acetylene, an intermediate.

The higher the TCE concentration, the higher the Fe^0 utilization efficiency for TCE dechlorination, which is evident from the decrease of H_2 evolution and the shift of byproduct formation toward an unsaturated byproduct (Liu et al. 2007), e.g., acetylene. At pH 7, 40% of Fe^0 in Fe^{H2} was consumed for H_2 production at a TCE concentration of 0.46 mM, while only 7% of the initial Fe^0 in Fe^{H2} was used for H_2 production at a TCE concentration of 8.4 mM (Liu et al. 2007). Evidently, TCE outcompeted Fe^0 with H^+. Similarly, acetylene accounted for 86% of the products, while ethene and ethane were 10% and 4%, respectively, at the TCE concentration of 8.4 mM (Liu et al. 2007). Acetylene formation requires fewer electrons than ethene and ethane formation, making TCE dechlorination by Fe^{H2} utilize electrons more effectively. The accumulation of acetylene could be the result of TCE saturating reactive sites and blocking acetylene from further transformation.

However, increasing the TCE concentration adversely affects the reactive life time of Fe^{H2}. The reactive lifetime of Fe^{H2} is 10, 40, and 60 days for TCE concentrations of 8.4, 1.3, and 0.46 mM, respectively, at pH 7 buffered by HEPES (Liu et al. 2007). At the DNAPL-water interface without HEPES, TCE dechlorination with Fe^{H2} decreased pH to 4–5. The reactive life time of Fe^{H2} at DNAPL interface was only 5 days, and no Fe^0 remained in the particles. The particle efficiency for TCE dechlorination using Fe^{H2} at the DNAPL-water interface was only ~15% because the local pH decreased and accelerated H_2 production in a much faster rate than increasing TCE dechlorination (see pH effect). This suggests that Fe^{H2} used for source zone treatment will have a relatively short lifetime. Therefore, additional injections for source zone treatment are expected to be more frequent than for plumes.

3.1.3.5 Microorganisms

Various kinds of microorganisms such as sulfate reducers, iron reducers, and methanogens are present under different geochemical conditions in the subsurface.

Some microorganisms such as halorespirers can biologically transform chlorinated organics to notorious byproducts under favorable conditions (Harkness et al. 1999; Cupples et al. 2004). Potential synergic effects of abiotic and biotic remediation via stimulated bioremediation using polymer-modified NZVI, leading to the long-term degradation of chlorinated organics, is an active area of research. Chapters 7 and 10 are devoted to this important combined remedy. The effects of microbes on NZVI reactivity and longevity are also discussed in Chap. 10. A reader should consult the microbiological-related materials in Chaps. 7 and 10 prior to designing an in situ remediation using NZVI since, in a real field implementation, interaction between NZVI and microbes is unavoidable and can substantially affect contaminant treatability.

3.2 Oxidative Transformation of Organic Contaminants Using NZVI-Induced Fenton's Reaction

While being considered a reducing agent, NZVI has also recently gained a lot of interest in the oxidation aspect. In general, NZVI can be used as a reagent in the process of producing oxidative radicals for contaminant degradation. Oxidation approaches of NZVI involve NZVI-induced Fenton's reaction (Xu and Wang 2011; Choi and Lee 2012; Li and Zhu 2014), NZVI under aeration (Taha and Ibrahim 2014a), and NZVI-induced persulfate system (Al-Shamsi and Thomson 2013; Diao et al. 2016). Nevertheless, the NZVI-induced Fenton's reaction is the most studied one. The state-of-the-art progress of the NZVI-induced Fenton's reaction is focused on in this section.

Discovered by Henry J. H. Fenton in 1894, Fenton's reaction is one of the most common chemical oxidation processes in wastewater treatment and site remediation (Ay and Kargi 2010; Petri et al. 2011; Babuponnusami and Muthukumar 2014; Papoutsakis et al. 2016). Typically, a homogeneous Fenton's reaction utilizes ferrous sulfate as a catalytic Fe^{2+} source. An acidic condition is required to maintain Fe^{2+} dissolution. However, acidification and the high dose of mobile ferrous/ferric required to obtain an effective treatment are the major drawbacks of conventional Fenton's reaction (Xu and Wang 2011; Li and Zhu 2014; Yu et al. 2014; Cheng et al. 2015; Usman et al. 2016). For in situ applications, the acidification of the subsurface is probably one of the most challenging problems due to the large buffering capacity at a neutral pH range of the aquifers (Petri et al. 2011). Moreover, acidification might result in the dissolution of metals in the subsurface (Petri et al. 2011). Hence, NZVI-induced Fenton's reaction has emerged as an alternative approach to avoid these problems.

3.2.1 Mechanism

The mechanism of contaminant degradation using NZVI-induced Fenton's reaction is primarily based on highly reactive radicals, which are generated from the reaction between Fe^0 and hydrogen peroxide. The radicals playing the key role in Fenton's reaction include highly reactive hydroxyl radical (•OH) and hydroperoxyl radical (OOH•). Instead of using acidification to maintain dissolved Fe^{2+} concentration, the NZVI Fenton process is self-catalytic, based on oxidative dissolution of NZVI in the presence of H_2O_2. Interfacial H^+ is produced at the NZVI surface to provide appropriate local pH, which continuously releases Fe^{2+} for Fenton's reaction. Babuponnusami and Muthukumar (2012), Chu et al. (2012), and Xu and Wang (2011) indicated the success of NZVI Fenton's reaction at circumneutral pH 6. Moreover, the NZVI Fenton process is more favorable than the conventional approach using dissolved Fe^{2+} because NZVI can be magnetically recovered and reused for several times (Diya'uddeen et al. 2015).

The critical reactions in a heterogeneous NZVI-induced Fenton's system are as follows:

$$Fe^0 + H_2O_2 + 2H^+ \rightarrow Fe^{2+} + 2H_2O \tag{3.13}$$

$$Fe^0 + O_2 + 2H^+ \rightarrow Fe^{2+} + H_2O_2 \tag{3.14}$$

$$Fe^0 + 2H^+ \rightarrow Fe^{2+} + H_2 \tag{3.15}$$

$$Fe^0 + H_2O \rightarrow Fe^{2+} + OH^- \tag{3.16}$$

$$Fe^{2+} + H_2O_2 \rightarrow Fe^{3+} + \cdot OH + OH^- \tag{3.17}$$

$$Fe^{2+} + \cdot OH \rightarrow Fe^{3+} + OH^- \tag{3.18}$$

$$Fe^{3+} + H_2O_2 \rightarrow Fe^{2+} + OOH \cdot + H^+ \tag{3.19}$$

The NZVI-induced Fenton's reaction has been reported to effectively degrade a variety of organic contaminants including textile wastewater, pharmaceuticals, halogenated compounds, and other non-halogenated compounds (Table 3.2). The degradation kinetics was found to fit well with the pseudo-first-order reaction. Degradation rates are mainly in the range of 0.01–0.2/min. However, depending on the reaction conditions, the rates can vary from 0.0064/min to 1.79/min. Zhang et al. (2017) reported that the degradation of norfloxacin was at a rate of 0.0064/min at pH 6, while the degradation rate at pH 3 was 0.1/min. Xu and Wang (2011) presented the 100% removal of 4-chloro-3-methyl phenol within 60 min at the degradation rate of 0.35/min at 0.1 g/L of NZVI and 1.79/min at 0.5 g/L of NZVI. In addition, although the NZVI-induced Fenton's reaction kinetics is pseudo-first-order in most of the cases, some studies suggest that the degradation kinetics is more appropriate for the pseudo-second-order reaction. For instance, Zhou et al. (2015) revealed the pseudo-second-order degradation of 1-alkyl-3-methylimidazolium-bromides at a rate of 0.0415 L/(mM·min).

Table 3.2 Summary of batch experiments for NZVI-induced Fenton's reaction of various organic contaminants

Contaminants	Optimal conditions	Degradation	Notes	References
Organic dyes				
Orange II	Orange II 105 mg/L; NZVI 0.02 g/L; H_2O_2 5.88 mM; pH 3	Orange II >95%; TOC 53%; reaction time 60 min	Pretreatment of NZVI reduction followed by Fenton oxidation improved degradation efficiency by 10%–15%	Moon et al. (2011)
Textile wastewater (reactive black B and polyvinyl alcohol)	COD 750–810 mg/L; NZVI 0.2–0.225 g/L; H_2O_2 30–33 mM; pH 2	COD 76%; reaction time 30 min	Wastewater was pretreated with NZVI reduction, followed by Fenton oxidation, and 10%–15% of COD was removed by NZVI reduction	Yu et al. (2014)
Halogenated compounds				
2,4-Dichlorophenoxyacetic acid (2,4-D)	2,4-D 235 mg/L; NZVI 0.6 g/L; H_2O_2 16.65 mM; pH 3	TOC 57%; reaction time 60 min	Employment of acoustic cavitation and hydrodynamic cavitation enhanced degradation efficiency by 5%–10%	Bremner et al. (2008)
4-Chlorophenol (4-CP)	4-CP 50–100 mg/L; NZVI 1–5 g/L; H_2O_2 0.016–0.065 mM; pH 3–4	Complete within 30 min; TOC 50%; $k = 0.35$–0.58/min	4-Chlorocatechol (4CC) and ortho-parachlorophenolperoxyl radical (ClPP•) were identified as intermediates and oxidized to aliphatic organic acids (e.g., maleic acid)	Zhou et al. (2008)
4-Chloro-3-methyl phenol (CMP)	CMP 50–150 mg/L; NZVI 0.1–0.5 g/L; H_2O_2 3.0 mM; pH 3.0–6.0	Complete within 60 min; $k = 0.35$–1.79/min	Two-stage reactions: Lag and degradation	Xu and Wang (2011)
Trichloroethylene (TCE)	TCE 70 mg/L; NZVI 8.5 g/L; H_2O_2 188 mM; pH 3.0–6.0; Cu (II) 20 mM	With cu(II): TCE 95% within 10 min $k = 4.90$/min Without cu (II): TCE 25% within 10 min	The presence of cu(II) could significantly enhanced the degradation of TCE by NZVI Fenton's reaction	Choi and lee (2012)

(continued)

Table 3.2 (continued)

Contaminants	Optimal conditions	Degradation	Notes	References
		$k = 0.0194$/min (at pH 3) $k = 0.0318$/min (at pH 6)		
p-chloro-nitroben-zene (p-ClNB)	p-ClNB 60 mg/L; NZVI 0.09–0.36 g/L; H_2O_2 4.9 mM; pH 2–3	Complete within 30 min; $k = 0.18$/min	Degradation was interfered by SO_4^{2-} 1 M, while the effects of Cl^- 1 M and NO_3^-1M were insignificant. Identified intermediates included azo compounds and aromatic amines. Carboxylic acids were the final products	Li and Zhu (2014)
4-Chlorophenol (4-CP)	4-CP 100 mg/L; NZVI 0.4 g/L; H_2O_2 9.79 mM; pH 3	Complete within 30 min	A presence of Cr(VI) that is greater than 10 mg/L slightly decreased the reaction rate due to Fe (II) consumption	Yin et al. (2014)
2,4-dichloro-phenol (2,4-DCP)	2,4-DCP 50–100 mg/L; NZVI 1.5–2.0 g/L; H_2O_2 10 mM; pH 3	2,4-DCP 88%–92%; TC 25%; TOC 30%; IC 10%; reaction time 180 min; $k = 0.022$–0.029/min	Higher temperatures (10–40 °C) produced higher degradation rates (0.022–0.084/min)	Li et al. (2015)
Chlorpheniramine	Chlorpheniramine 5–15 mg/L; NZVI 22.4 g/L; H_2O_2 0.1 mM; pH 2–3	Complete within 60 min; TOC 21%; $k = 0.093$/min	4-hydroxy-4-methyl-2-pentanone, 2-methylaminopyridine, and NDMA were identified as interme-diates that were resistant to the treatment	Wang et al. (2016b)
Non-halogenated compounds				
Phenol	Phenol 100–400 mg/L; NZVI 0.5 g/L; H_2O_2 14.7 mM; pH 2–6.2 (natural pH); current density 12 mA/cm^2; an 8 W UV lamp ($\lambda = 254$ nm)	Complete within 60 min; $k = 0.0926$/min	Assisted with photo-electro effect	Babuponnusami and Muthukumar (2012)

Palm oil mill effluent	COD 1160 mg/L; NZVI 0.6 g/L; H_2O_2 40 mM; pH 2; Ultrasound 20 kHz	COD 80%; reaction time 120 min	The employment of an ultrasound accelerated the degradation from 24 h (in silence) to 2 h	Taha and Ibrahim (2014a)
Palm oil mill effluent	COD 4568 mg/L; NZVI 3.91 g/L; H_2O_2 54 mM; pH 2; Aeration rate 23.84 L/min	COD up to 71%; reaction time 240 min	The employment of aeration improved the degradation efficiency by 10-20%	Taha and Ibrahim (2014b)
Petroleum refinery wastewater	COD 1259 mg/L; BOD 173 mg/L; Phenol 14.7 mg/L; Oil and grease 233 mg/L; NZVI 1.24 g/L; H_2O_2 222 mM; pH 3	COD 76.5%; BOD 37.6%; TOC 45% phenol 96%; oil and grease 100%; reaction time 120 min	Followed by sequencing batch reactor (SBR). Fenton's process improved the biodegradability of the wastewater for SBR treatment. The BOD_5/COD ratio increased from 0.137 to 0.365, while approx. 130 mg/L of total iron was produced after Fenton's process	Diya'uddeen et al. (2015)
Naphthalene	Naphthalene 200 mg/L; NZVI 1.0 g/L; H_2O_2 10 mM; pH 3	COD 82.7%; reaction time 60 min	The wastewater was pretreated with bacterial strains of Bacillus fusiformis (BFN) for 40 h, followed by Fenton's oxidation	Yu et al. (2015)
1-Alkyl-3-methyl-imidazolium-bromides ([$C_n$mim]Br)	[C_4mim]Br 438 mg/L; NZVI 0.25–1.0 g/L; H_2O_2 40–100 mM; pH 3–4; ultrasound 45 kHz	[$C_n$mim]Br 80%-90%; reaction time 120 min; $k = 0.0415$ L/(mM.min)	Assisted with ultrasound	Zhou et al. (2015)
Phenol	Phenol 25 mg/L; NZVI 1.0 g/L; H_2O_2 30 mM; pH 7; ultrasound 20 kHz	Phenol 75%; reaction time 60 min; $k = 0.0145$/min	Assisted with ultrasonic irradiation	Yehia et al. (2015)
Pharmaceuticals, personal care products, and microbial toxins				
Amoxicillin (AMX)	AMX 50 mg/L; NZVI 0.5 g/L; H_2O_2 6.6 mM; pH 3–4	AMX 86%; reaction time 20 min; $k = 0.15$/min	The degradation was affected by temperature. At 45 °C, H_2O_2 tends to be decomposed	Zha et al. (2014)

(continued)

Table 3.2 (continued)

Contaminants	Optimal conditions	Degradation	Notes	References
Norfloxacin (NOR)	NOR 100 mg/L; NZVI 0.1 g/L; H_2O_2 20 mM; pH 3	NOR 95%; TOC 50%; reaction time 40 min; $k = 0.10$/min (pH 3); $k = 0.063$/min (pH 5); $k = 0.0064$/min (pH 6)	The optimal temperature was 25–35 °C. At either lower or higher temperature, the degradation tends to be inhibited	Zhang et al. (2017)
Microcystin-LR (MC-LR)	MC-LR 5 mg/L; NZVI 0.6 g/L; H_2O_2 6.6 mM; pH 6.86	MC-LR 59.1%; COD 22%; reaction time 250 min; $k = 0.14$/min	The presence of humic acid and oxalate enhanced the degradation efficiency by 10–20%	Wang et al. (2016a)

In general, NZVI-induced Fenton's reaction has high reactivity. However, it is a two-stage reaction, in which the first stage usually shows low degradation rates and is followed by a rapid degradation in the second stage. The lag stage is considered an activation process of the surface iron species where iron dissolution occurs on the NZVI surface and participates in the catalytic reaction. Moreover, despite the high reactivity, the degradation by NZVI-induced Fenton's reaction is usually inhibited quickly ranging from 0.5 to 3 h due to the depletion of H_2O_2. Yu et al. (2014) showed that the textile wastewater removal was inhibited after 40 min gaining 80% efficiency. Cheng et al. (2015) reported the inhibition of pentachlorophenol degradation after an hour with a removal efficiency of 60%. Zha et al. (2014) described that amoxicillin degradation was impeded after 15 min, obtaining approximately 80% removal efficiency. The inhibition even occurs more frequently at a neutral pH (Li and Zhu 2014; Zhou et al. 2015; Wang et al. 2016b). The sequential addition of Fenton's reagent can be a solution to this problem. Munoz et al. (2014) presented the prolongation of homogenous Fenton reaction to treat sawmill wastewater by the sequential addition of H_2O_2.

3.2.2 Factors Affecting Treatment Efficiency

3.2.2.1 Reagent Dose

The H_2O_2 acts as a scavenger of hydroxyl radical (OH) (Xu and Wang 2011; Li and Zhu 2014; Li et al. 2015; Wang et al. 2016b) as shown in Eqs. 3.20 and 3.21, while ·OH plays the dominant role in contaminant degradation (Petri et al. 2011). In addition, H_2O_2 can be self-degraded as presented in Eq. 3.22. Therefore, the use of excessive H_2O_2 led to the degradation inefficiency. As a result, sequential H_2O_2 addition, as done in the homogeneous Fenton's process (Martins et al. 2010; Villa et al. 2010; Munoz et al. 2014), is also a possible solution for sustaining NZVI-induced Fenton's reaction as to be discussed next in the treatability of 1,2-DCA.

$$H_2O_2 + \cdot OH \rightarrow HO_2 \cdot + H_2O \tag{3.20}$$

$$HO_2 \cdot + \cdot OH \rightarrow H_2O + O_2 \tag{3.21}$$

$$H_2O_2 + H_2O_2 \rightarrow 2H_2O + O_2 \tag{3.22}$$

$$Fe^{2+} + H_2O_2 \rightarrow Fe^{3+} + \cdot OH + OH^- \tag{3.24}$$

$$Fe^{2+} + \cdot OH \rightarrow Fe^{3+} + OH^- \tag{3.25}$$

The NZVI was the source to generate ·OH (Li et al. 2015; Wang et al. 2016b) as shown in Eqs. 3.13 and 3.24. Therefore, a higher NZVI concentration provided higher degradation efficiency. However, the excessive iron source has been known as an ·OH scavenger (Xu and Wang 2011; Wang et al. 2016b), which may prohibit

the degradation as shown in Eqs. 3.13 and 3.25. Table 3.2 summarizes the optimal reagent dose and conditions for the treatment of various contaminants.

3.2.2.2 Initial pH

Babuponnusami and Muthukumar (2012) and Xu and Wang (2011) also reported that the heterogeneous NZVI Fenton's reaction at a neutral pH succeeded in removing phenol and 4-chloro-3-methyl phenol, respectively. Babuponnusami and Muthukumar (2012) reported 65% of phenol removal using NZVI Fenton's process at a pH 6.2. Chu et al. (2012) showed a decrease of 95% in total phenols and 50% in COD of coking wastewater using iron powder as a Fenton's catalyst at pH 6.5 and 5.4. Xu and Wang (2011) presented the complete degradation of 4-chloro-3-methyl phenol using an NZVI-induced Fenton's system at a pH of 6.1. Some examples of optimal pH values for the treatment of different organic contaminants are summarized in Table 3.2.

3.2.3 Treatability of 1,2–DCA

While reductive dechlorination using NZVI is incapable of detoxifying 1,2-DCA as discussed previously, the Fenton process can. Masten and Butler (1986) suggested the success of 1,2-DCA degradation due to free radicals. Noticeably, Vilve et al. (2010) successfully degraded 1,2-DCA at the laboratory scale using a conventional Fenton process. Recently, Le and Phenrat (2018) evaluated the NZVI-induced Fenton process at a neutral pH to degrade 1,2-DCA at a high concentration (2000 mg/L), representing a dissolved 1,2-DCA concentration close to the DNAPL source zone. Approximately 87% of 1,2-DCA was degraded at a neutral pH, with a pseudo-first-order rate constant of 0.98/h using 10 g/L of NZVI and 200 mM of H_2O_2. However, the reaction was prohibited quickly, within 3 h, presumably due to the rapid depletion of H_2O_2. The application of sequential H_2O_2 addition provided a better approach for preventing rapid inhibition via controlling the H_2O_2 concentration in the system to be sufficient but not in excess, thus resulting in the higher degradation efficiency (the pseudo-first-order rate constant of 0.49/h and 99% degradation in 8 h for 10 g/L NZVI and 200 mM but sequential for 25 mM per 30 min). Using NZVI with sequential H_2O_2 addition (25 mM per 30 min) was also successful in degrading 1,2-DCA sorbed onto soil, yielding 99% removal of 1,2-DCA within 16 h at a rate constant of 0.23/h (Fig. 3.13a), around two times slower than in the system without soil, presumably due to rate-limited 1,2-DCA desorption from the soil.

The NZVI-induced Fenton reaction can be reused for several treatment cycles. Figure 3.13b illustrates the 1,2-DCA degradation kinetics using NZVI-induced Fenton's reaction in three consecutive cycles. In the first cycle of degradation, 99.9% of 1,2-DCA was degraded for 16 h, obtaining the rate constant of 0.49/h.

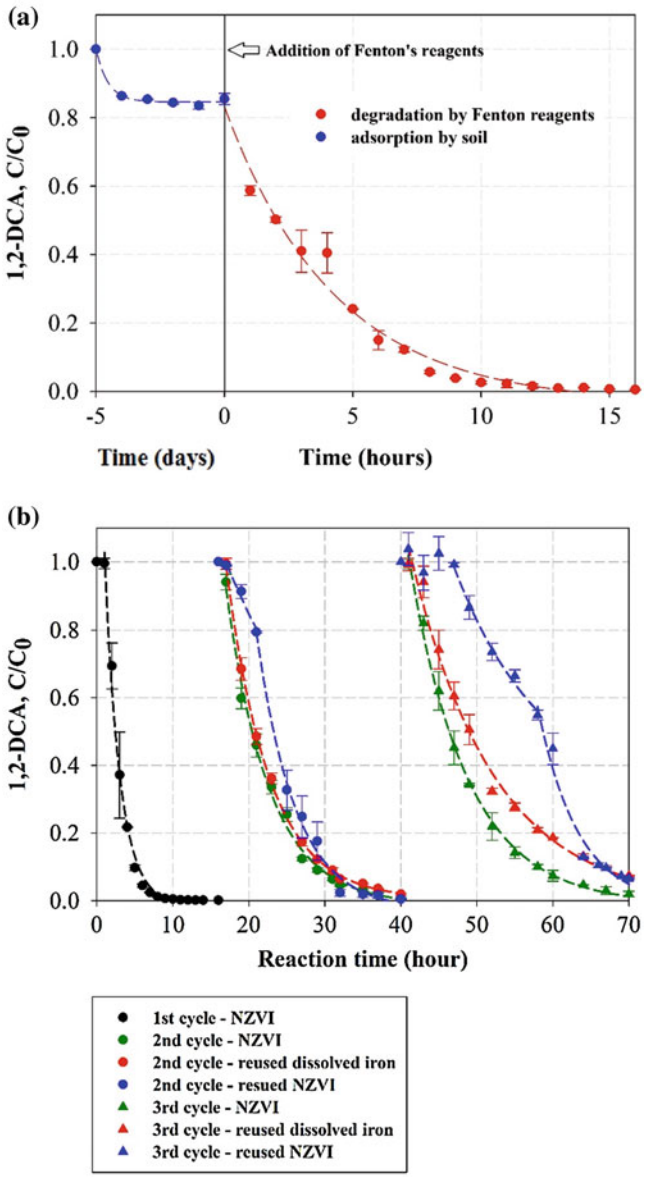

Fig. 3.13 (**a**) 1,2-DCA degradation in soil-groundwater system and (**b**) NZVI reuse for three removal cycles (conditions: natural pH, initial 1,2-DCA 2000 mg/L, NZVI 10 g/L, 25 mM H_2O_2 per 30 min)

When the stock 1,2-DCA solution was added into the reactors to restart the treatment cycles, the degradation rate constant declined almost three times to 0.18/h in Cycle 2 and four times to 0.13/h in Cycle 3. Approximately 99.2% and 98.0% of 1,2-DCA

were degraded for 24 h and 30 h in Cycles 2 and 3, respectively. This finding suggests that the heterogeneous NZVI Fenton process is a promising approach for in situ treatment. The NZVI can be emplaced in the subsurface close to the DNAPL source zone, while a small amount of H_2O_2 is recirculated to treat 1,2-DCA in both groundwater and soil.

References

Al-Shamsi, M. A., & Thomson, N. R. (2013). Treatment of organic compounds by activated persulfate using nanoscale zerovalent iron. *Industrial & Engineering Chemistry Research, 52*, 13564–13571.

Amir, A., & Lee, W. (2011). Enhanced reductive dechlorination of tetrachloroethene by nano-sized zerovalent iron with vitamin B12. *Chemical Engineering Journal, 170*, 492–497.

Arnold, W. A., & Roberts, A. L. (2000). Pathway and kinetics of chlorinated ethylene and chlorinated acetylene reaction with Fe(0) particles. *Environmental Science & Technology, 34*, 1794–1805.

Ay, F., & Kargi, F. (2010). Advanced oxidation of amoxicillin by Fenton's reagent treatment. *Journal of Hazardous Materials, 179*, 622–627.

Babuponnusami, A., & Muthukumar, K. (2012). Removal of phenol by heterogenous photo electro Fenton-like process using nano-zero valent iron. *Separation and Purification Technology, 98*, 130–135.

Babuponnusami, A., & Muthukumar, K. (2014). A review on Fenton and improvements to the Fenton process for wastewater treatment. *Journal of Environmental Chemical Engineering, 2*, 557–572.

Baer, D. R., Tratnyek, P. G., Qiang, Y., Amonette, J. E., Linehan, J., Sarathy, V., Nurmi, J. T., Wang, C.-M., & Antony, J. (2007). Synthesis, characterization, and properties of zero-valent iron nanoparticles. In G. E. Fryxell & G. Cao (Eds.), *Environmental applications of nanomaterials*. London: Imperial College Press.

Berge, N. D., & Ramsburg, C. A. (2010). Iron-mediated trichloroethene reduction within nonaqueous phase liquid. *Journal of Contaminant Hydrology, 118*, 105–116.

Bremner, D. H., Carlo, S. D., Chakinala, A. G., & Cravotto, G. (2008). Mineralisation of 2,4-dichlorophenoxyacetic acid by acoustic or hydrodynamic cavitation in conjunction with the advanced Fenton process. *Ultrasonics Sonochemistry, 15*, 416–419.

Cao, J., Xu, R., Tang, H., Tang, S., & Cao, M. (2011). Synthesis of monodispersed CMC-stabilized Fe–Cu bimetal nanoparticles for in situ reductive dechlorination of 1, 2, 4-trichlorobenzene. *The Science of the Total Environment, 409*, 2336–2341.

Chen, J., Xiu, Z., Lowry, G. V., & Alvarez, P. (2011a). Effect of natural organic matter on toxicity and reactivity of nano-scale zero-valent iron. *Water Research, 45*, 1995–2001.

Chen, Z.-X., Jin, X.-Y., Chen, Z., Megharaj, M., & Naidu, R. (2011b). Removal of methyl orange from aqueous solution using bentonite-supported nanoscale zero-valent iron. *Journal of Colloid and Interface Science, 363*, 601–607.

Cheng, R., Cheng, C., Liu, G. H., Zheng, X., Li, G., & Li, J. (2015). Removing pentachlorophenol from water using a nanoscale zero-valent iron/H2O2 system. *Chemosphere, 141*, 138–143.

Cho, H.-H., & Park, J. W. (2006). Sorption and reduction of tetrachloroethylene with zero valent iron and amphiphilic molecules. *Chemosphere, 64*, 1047–1052.

Choi, K., & Lee, W. (2012). Enhanced degradation of trichloroethylene in nano-scale zero-valent iron Fenton system with Cu(II). *Journal of Hazardous Materials, 211-212*, 146–153.

Choi, H., Al-Abed, S. R., Agarwal, S., & Dionysiou, D. (2008). Synthesis of reactive Nano-Fe/Pd bimetallic system-impregnated activated carbon for the simultaneous adsorption and dechlorination of PCBs. *Chemistry of Materials, 20*, 3649–3655.

Chu, L., Wang, J., Dong, J., Liu, H., & Sun, X. (2012). Treatment of coking wastewater by an advanced Fenton oxidation process using iron powder and hydrogen peroxide. *Chemosphere, 86*, 409–414.

Cioslowski, J., Liu, G., & Moncrieff, D. (1997). Thermochemistry of homolytic C-C, C-H, and C-Cl bond dissociations in polychloroethanes: benchmark electronic structure calculations. *Journal of the American Chemical Society, 119*, 11452–114757.

Cupples, A. M., Spormann, A. M., & McCarty, P. L. (2004). Comparative evaluation of chloroethene dechlorination to ethene by dehalococcoides-like microorganisms environ. *Science and Technology, 38*, 4768–4774.

Deng, B., & Hu, S. (2007). Reductive dechlorination of chlorinated solvents on zerovalent iron surfaces. In J. A. Smith & S. E. Burns (Eds.), *Physicochemical Groundwater Remediation* (pp. 139–160). New York: Springer Science & Business Media.

Diao, Z. H., Xu, X. R., Chen, H., Jiang, D., Yang, Y. X., Kong, L. J., Sun, Y. X., Hu, Y. X., Hao, Q. W., & Liu, L. (2016). Simultaneous removal of Cr(VI) and phenol by persulfate activated with bentonite-supported nanoscale zero-valent iron: Reactivity and mechanism. *Journal of Hazardous Materials, 316*, 186–193.

Diya'uddeen, B. H., Rahim Pouran, S., Abdul Aziz, A. R., Nashwan, S. M., Wan Daud, W. M. A., & Shaaban, M. G. (2015). Hybrid of Fenton and sequencing batch reactor for petroleum refinery wastewater treatment. *Journal of Industrial and Engineering Chemistry, 25*, 186–191.

Dong, H., Zhao, F., Zeng, G., Tang, L., Fan, C., Zhang, L., Zeng, Y., He, Q., Xie, Y., & Wu, Y. (2016). Aging study on carboxymethyl cellulose-coated zero-valent iron nanoparticles in water: Chemical transformation and structural evolution. *Journal of Hazardous Materials, 312*, 234–242.

Doong, R.-A., & Lai, Y.-L. (2006). Effect of metal ions and humic acid on the dechlorination of tetrachloroethylene by zerovalent iron. *Chemosphere, 64*, 371–378.

Dries, J., Bastiaens, L., Springael, D., Agathos, S. N., & Diels, L. (2005). Combined removal of chlorinated ethenes and heavy metals by zerovalent iron in batch and continuous flow column systems environ. *Science and Technology, 39*, 8460–8465.

Elliott, D. W., Lien, H.-L., & Zhang, W. X. (2009). Degradation of lindane by zero-valent iron nanoparticles. *Journal of Environmental Engineering, 135*, 317–324.

Fagerlund, F., Illangasekare, T. H., Phenrat, T., Kim, H. J., & Lowry, G. V. (2012). PCE dissolution and simultaneous dechlorination by nanoscale zero-valent iron particles in a DNAPL source zone. *Journal of Contaminant Hydrology, 131*, 9–28.

Fleer, G. J., Cohen Stuart, M. A., Scheutjens, J. M. H. M., Cosgrove, T., & Vincent, B. (1998). *Polymers at interfaces*. New York: Chapman & Hall.

Frost, R. L., Xi, Y., & He, H. (2010). Synthesis, characterization of palygorskite supported zero-valent iron and its application for methylene blue adsorption. *Journal of Colloid and Interface Science, 341*, 153–161.

Garcia, A. N., Boparai, H. K., & O'Carroll, D. M. (2016). Enhanced Dechlorination of 1,2-Dichloroethane by coupled Nano Iron-dithionite treatment. *Environmental Science & Technology, 50*, 5243–5251.

Ghosh, C. K. (2015). Quantum effect on properties of nanomaterials. In A. Sengupta & C. K. Sarkar (Eds.), *Introduction to nano: Basics to nanoscience and nanotechnology* (pp. 73–111). Berlin/Heidelberg: Springer.

Gillham, R. W., & O'Hannesin, S. F. (1994). Enhanced degradation of halogenated aliphatics by zero-valent iron. *Groundwater, 32*, 958–967.

Han, L., Xue, S., Zhao, S., Yan, J., Qian, L., & Chen, M. (2015). Biochar supported nanoscale iron particles for the efficient removal of methyl orange dye in aqueous solutions. *PLoS One, 10*, e0132067.

Harkness, M. R., Bracco, A. A., Brennan, M. J., Jr., DeWeerd, K. A., & Spivack, J. L. (1999). Use of bioaugmentation to stimulate complete reductive dechlorination of trichloroethene in dover soil columns environ. *Science and Technology, 33*, 1100–1109.

He, F., & Zhao, D. (2005). Preparation and characterization of a new class of starch-stabilized bimetallic nanoparticles for degradation of chlorinated hydrocarbons in water. *Environmental Science & Technology, 39*, 3314–3320.

He, F., & Zhao, D. (2008). Hydrodechlorination of trichloroethene using stabilized Fe-Pd nanoparticles: Reaction mechanism and effects of stabilizers, catalysts, and reaction conditions. *Applied Catalysis B: Environmental, 84*, 533–540.

He, F., Zhao, D., Liu, J., & ROberts, C. B. (2007). Stabilization of Fe−Pd nanoparticles with sodium Carboxymethyl cellulose for enhanced transport and Dechlorination of trichloroethylene in soil and groundwater. *Industrial and Engineering Chemistry Research, 46*, 29–34.

Hepure Technology Inc. (2017). *Technical specification sheet: Ferox flow ZVI reactive iron powder*. Flemington: Hepure Technology.

Huang, Q., Liu, W., Peng, P., & Huang, W. (2013). Reductive debromination of tetrabromobisphenol A by Pd/Fe bimetallic catalysts. *Chemosphere, 92*, 1321–1327.

Hyung, H., Fortner, J. D., Hughes, J. B., & Kim, J. H. (2007). Natural organic matter stabilizes carbon nanotubes in the aqueous phase. *Environmental Science & Technology, 41*, 179–184.

Jia, H., & Wang, C. (2015). Dechlorination of chlorinated phenols by subnanoscale Pd0/Fe0intercalated in smectite: Pathway, reactivity, and selectivity. *Journal of Hazardous Materials, 300*, 779–787.

Jiang, Q., Liang, L. H., & Zhao, D. S. (2001). Lattice contraction and surface stress of fcc nanocrystals. *The Journal of Physical Chemistry B, 105*, 6275–6277.

Johnson, T. L., Scherer, M. M., & Tratnyek, P. G. (1996). Kinetics of halogenated organic compound degradation by iron metal. *Environmental Science & Technology, 30*, 2634–2640.

Kanel, S. R., Manning, B., Charlet, L., & Choi, H. (2005). Removal of arsenic(III) from groundwater by nanoscale zero-valent iron. *Environmental Science & Technology, 39*, 1291–1298.

Kim, H.-S., Kim, T., Ahn, J.-Y., Hwang, K.-Y., Park, J.-Y., Lim, T.-T., & Hwang, I. (2012). Aging characteristics and reactivity of two types of nanoscale zero-valent iron particles (FeBH and FeH2) in nitrate reduction. *Chemical Engineering Journal, 197*, 16–23.

Kim, H. J., Leitch, M., Naknakorn, B., Tilton, R. D., & Lowry, G. V. (2017). Effect of emplaced nZVI mass and groundwater velocity on PCE dechlorination and hydrogen evolution in water-saturated sand. *Journal of Hazardous Materials, 322*, 136–144.

Li, X.-Q., & Zhang, W.-X. (2007). Sequestration of metal cations with zerovalent iron nanoparticles-a study with high resolution X-ray photoelectron spectroscopy (HR-XPS) J. *Physical Chemistry C, 111*, 6939–6946.

Li, B., & Zhu, J. (2014). Removal of p-chloronitrobenzene from groundwater: Effectiveness and degradation mechanism of a heterogeneous nanoparticulate zero-valent iron (NZVI)-induced Fenton process. *Chemical Engineering Journal, 255*, 225–232.

Li, R., Gao, Y., Jin, X., Chen, Z., Megharaj, M., & Naidu, R. (2015). Fenton-like oxidation of 2,4-DCP in aqueous solution using iron-based nanoparticles as the heterogeneous catalyst. *Journal of Colloid and Interface Science, 438*, 87–93.

Li, Y., Li, X., Xiao, Y., Wei, C., Han, D., & Huang, W. (2016). Catalytic debromination of tetrabromobisphenol A by Ni/nZVI bimetallic particles. *Chemical Engineering Journal, 284*, 1242–1250.

Li, Y., Li, X., Han, D., Huang, W., & Yang, C. (2017). New insights into the role of Ni loading on the surface structure and the reactivity of nZVI toward tetrabromo- and tetrachlorobisphenol A. *Chemical Engineering Journal, 311*, 173–182.

Lien, H.-L., & Zhang, W. X. (1999). Transformation of chlorinated methanes by nanoscale Iron particles. *Journal of Environmental Engineering, 125*, 1042–1047.

Lien, H.-L., & Zhang, W. X. (2001). Nanoscale iron particles for complete reduction of chlorinated ethenes. *Colloids and Surfaces A, 191*, 97–105.

Lien, H.-L., & Zhang, W. X. (2005). Hydrodechlorination of chlorinated ethanes by nanoscale Pd/Fe bimetallic particles. *Journal of Environmental Engineering, 131*, 4–10.

Liu, Y., & Lowry, G. V. (2006). Effect of particle age (Fe0 content) and solution pH on NZVI reactivity: H2 evolution and TCE dechlorination. *Environmental Science & Technology, 40*, 6085–6090.

Liu, Y., Choi, H., Dionysiou, D., & Lowry, G. V. (2005a). Trichloroethene hydrodechlorination in water by highly disordered monometallic nanoiron. *Chemistry of Materials, 17*, 5315–5322.

Liu, Y., Majetich, S. A., Tilton, R. D., Sholl, D. S., & Lowry, G. V. (2005b). TCE dechlorination rates, pathways, and efficiency of nanoscale iron particles with different properties. *Environmental Science & Technology, 39*, 1338–1345.

Liu, Y., Phenrat, T., & Lowry, G. V. (2007). Effect of TCE concentration and dissolved groundwater solutes on NZVI-promoted TCE dechlorination and H2 evolution. *Environmental Science & Technology, 41*, 7881–7887.

Liu, A., Liu, J., & Zhang, W. X. (2015). Transformation and composition evolution of nanoscale zero valent iron (nZVI) synthesized by borohydride reduction in static water. *Chemosphere, 119*, 1068–1074.

Le, T. S. T., & Phenrat, T. (2018). Sustaining 1,2-Dichloroethane Degradation in Nanoscale Zero-Valent Iron induced Fenton System by Using Sequential H2O2 Addition at Natural pH. Water Research, (Under Review).

Mackenzie, K., Bleyl, S., Georgi, A., & Kopinke, F.-D. (2012). Carbo-Iron – An Fe/AC composite – As alternative to nano-iron for groundwater treatment. *Wat. Res., 46*, 3817–3826.

Maes, A., Reamdinck, H. V., Smith, K., Ossieur, W., Lebbe, L., & Verstraete, W. (2006). Transport and activity of desulfitobacterium dichloroeliminans strain DCA1 during bioaugmentation of 1,2-DCA-contaminated groundwater. *Environmental Science and Technology, 40*, 5544–5552.

Martins, R. C., Rossi, A. F., & Quinta-Ferreira, R. M. (2010). Fenton's oxidation process for phenolic wastewater remediation and biodegradability enhancement. *Journal of Hazardous Materials, 180*, 716–721.

Masten, S. J., & Butler, J. N. (1986). Ultraviolet-enhanced ozonation of organic compounds: 1,2-Dichloroethane and trichloroethylene as model substrates. *Ozone: Science & Engineering, 8*, 339–353.

Mccormick, M. L., & Adriaens, P. (2004). Carbon tetrachloride transformation on the surface of nanoscale biogenic magnetite particles. *Environmental Science & Technology, 38*, 1045–1053.

Moon, B.-H., Park, Y.-B., & Park, K.-H. (2011). Fenton oxidation of Orange II by pre-reduction using nanoscale zero-valent iron. *Desalination, 268*, 249–252.

Munoz, M., Pliego, G., de Pedro, Z. M., Casas, J. A., & Rodriguez, J. J. (2014). Application of intensified Fenton oxidation to the treatment of sawmill wastewater. *Chemosphere, 109*, 34–41.

Naja, G., Halasz, A., Thiboutot, S., Ampleman, G., & Hawari, J. (2008). Degradation of hexahydro-1,3,5-trinitro-1,3,5-triazine (RDX) using zerovalent iron nanoparticles. *Environmental Science & Technology, 42*, 4364–4370.

Nurmi, J. T., Tratnyek, P. G., Sarathy, V., Baer, D. R., Amonette, J. E., Pecher, K., Wang, C., Linehan, J. C., Matson, D. W., Penn, R. L., & Driessen, M. D. (2005). Characterization and properties of metallic iron nanoparticles: Spectroscopy, electrochemistry, and kinetics. *Environmental Science & Technology, 39*, 1221–1230.

Papoutsakis, S., Pulgarin, C., Oller, I., Sánchez-Moreno, R., & Malato, S. (2016). Enhancement of the Fenton and photo-Fenton processes by components found in wastewater from the industrial processing of natural products: The possibilities of cork boiling wastewater reuse. *Chemical Engineering Journal, 304*, 890–896.

Petri, B. G., Watts, R. J., Teel, A. L., & Hugling, S. G. (2011). Fundamentals of ISCO using hydrogen peroxide. In R. L. Siegrist, M. Crimi, & T. L. Simpkin (Eds.), *Situ chemical oxidation for groundwater remediation* (pp. 33–88). New York: Springer Science+Business Media, LLC.

Phenrat, T., Kim, H.-J., Fagerlund, F., Illangasekare, T., Tilton, R. D., & Lowry, G. V. (2009a). Particle size distribution, concentration, and magnetic attraction affect transport of polymer-modified Fe^0 nanoparticles in sand columns. *Environmental Science & Technology, 43*, 5079–5085.

Phenrat, T., Liu, Y., Tilton, R. D., & Lowry, G. V. (2009b). Adsorbed polyelectrolyte coatings decrease Fe^0 nanoparticle reactivity with TCE in water: Conceptual model and mechanisms. *Environmental Science & Technology, 43*, 1507–1514.

Phenrat, T., Schoenfelder, D., Kirschling, T. L., Tilton, R. D., Lowry, G. V. (2015). Adsorbed poly (aspartate) coating limits the adverse effects of dissolved groundwater solutes on Fe^0 nanoparticle reactivity with trichloroethylene. *Environmental Science Pollution Research Vol 25* (8) 7157–7169.

Phenrat, T., Thongboot, T., & Lowry, G. V. (2016). Electromagnetic induction of zerovalent iron (ZVI) powder and nanoscale zerovalent iron (NZVI) particles enhances dechlorination of trichloroethylene in contaminated groundwater and soil: Proof of concept. *Environmental Science & Technology, 50*, 872–880.

Ponder, S. M., Darab, J. G., & Mallouk, T. E. (2000). Remediation of Cr(VI) and Pb(II) aqueous solutions using supported, nanoscale zero-valent Iron. *Environmental Science & Technology, 34*, 2564–2569.

Ramos-Tejada, M. M., Ontiveros, A., Viota, J. L., & Durán, J. D. G. (2003). Interfacial and rheological properties of humic acid/hematite suspensions. *Journal of Colloid and Interface Science, 268*, 85–95.

Reinsch, B. C., Forsberg, B., Penn, R. L., Kim, C. S., & Lowry, G. V. (2010). Chemical transformations during aging of zero-valent iron nanoparticles in the presence of common groundwater dissolved constituents. *Environmental Science & Technology, 44*, 3455–3461.

Reynolds, G. W., Hoff, J. T., & Gillham, R. W. (1990). Sampling bias caused by materials used to monitor halocarbons in groundwater. *Environmental Science & Technology, 24*, 135–142.

Sakulchaicharoen, N., O'Carroll, D. M., & Herrera, J. E. (2010). Enhanced stability and dechlorination activity of pre-synthesis stabilized nanoscale FePd particles. *Journal of Contaminant Hydrology, 118*, 117–127.

Sarathy, V., Tratnyek, P. G., Nurmi, J. T., Baer, D. R., Amonette, J. E., Chun, C. L., Penn, R. L., & Reardon, E. J. (2008). Aging of iron nanoparticles in aqueous solution: Effects on structure and reactivity. *Journal of Physical Chemistry C, 112*, 2286–2293.

Scheutjens, J. M. H. M., & Fleer, G. J. (1979). Statistical theory of the adsorption of interacting chain molecules. 1. Partition function, segment density distribution, and adsorption isotherms. *The Journal of Physical Chemistry, 83*, 1619–1635.

Scheutjens, J. M. H. M., & Fleer, G. J. (1980). Statistical theory of the adsorption of interacting chain molecules. 2. Train, loop, and tail size distribution. *The Journal of Physical Chemistry, 84*, 178–190.

Schlicker, O., Ebert, M., Fruth, M., Weidner, M., Wust, W., & Dahmke, A. (2000). Degradation of TCE with iron: The role of competing chromate and nitrate reduction. *Groundwater, 38*, 403–409.

Schrick, B., Blough, J. L., Jones, A. D., & Mallouk, T. E. (2002). Hydrodechlorination of trichloroethylene to hydrocarbons using bimetallic nickel-iron nanoparticles. *Chemistry of Materials, 14*, 5140–5147.

Schwarzenbach, R. P., Gschwend, P. M., & Imboden, D. M. (2003a). *Environmental organic chemistry* (2nd ed.). Hoboken: Wiley.

Schwarzenbach, R. P., Gschwend, P. M., & Imboden, D. M. (2003b). *Environmental organic chemistry* (2nd ed.). Hoboken: Wiley-Interscience.

Shih, Y.-H., Chen, Y.-C., Chen, M.-Y., Tai, Y.-T., & Tso, C.-P. (2009). Dechlorination of hexachlorobenzene by using nanoscale Fe and nanoscale Pd/Fe bimetallic particles. *Colloids and Surfaces A, 332*, 84–89.

Shu, H.-Y., Chang, M.-C., Chen, C.-C., & Chen, P.-E. (2010). Using resin supported nano zero-valent iron particles for decoloration of acid blue 113 azo dye solution. *Journal of Hazardous Materials, 184*, 499–505.

Song, H., & Carraway, E. R. (2005). Reduction of chlorinated ethanes by nanosized zero-valent iron: Kinetics, pathways, and effects of reaction conditions. *Environmental Science & Technology, 39*, 6237–6245.

Song, H., & Carraway, E. R. (2006). Reduction of chlorinated methanes by nano-sized zero-valent Iron. Kinetics, pathways, and effect of reaction conditions. *Environmental Engineering Science, 23*, 272–284.

Su, C., Puls, R. W., Krug, T. A., Watling, M. T., O'Hara, S. K., Quinn, J. W., & Ruiz, N. W. (2012a). A two and half-year-performance evaluation of a field test on treatment of source zone tetrachloroethene and its chlorinated daughter products using emulsified zero valent iron nanoparticles. *Water Research, 46*, 5071–5084.

Su, Y.-F., Hsu, C.-Y., & Shih, Y.-H. (2012b). Effects of various ions on the dechlorination kinetics of hexachlorobenzene by nanoscale zero-valent iron. *Chemosphere, 88*, 1346–1352.

Sun, Y.-P., Li, X.-Q., Zhang, W. X., & Wang, H. P. (2007). A method for the preparation of stable dispersion of zero-valent iron nanoparticles. *Colloids and Surfaces A, 308*, 60–66.

Scherer, M. M., Balko, B. A., Gallagher, D. A., Tratnyek, P. G. (1998). Correlation Analysis of Rate Constants for Dechlorination by Zero-Valent Iron. Environmental Science Technology, 32 (19), 3026–3033

Taha, M. R., & Ibrahim, A. H. (2014a). Characterization of nano zero-valent iron (nZVI) and its application in sono-Fenton process to remove COD in palm oil mill effluent. *Journal of Environmental Chemical Engineering, 2*, 1–8.

Taha, M. R., & Ibrahim, A. H. (2014b). COD removal from anaerobically treated palm oil mill effluent (AT-POME) via aerated heterogeneous Fenton process: Optimization study. *Journal of Water Process Engineering, 1*, 8–16.

Thompson, J. M., Chrisholm, B. J., & Bezbaruah, A. N. (2010). Reductive dechlorination of chloroacetanilide herbicide (Alachlor) using zero-valent iron nanoparticles. *Environmental Engineering Science, 27*, 227–232.

Tobiszewski, M., & Namieśnik, J. (2012). Abiotic degradation of chlorinated ethanes and ethenes in water. *Environmental Science and Pollution Research, 19*, 1994–2006.

Totten, L. A., & Roberts, A. L. (2010). Calculated one- and two-electron reduction potentials and related molecular descriptors for reduction of alkyl and vinyl halides in water. *Critical Reviews in Environment Science and Technology, 31*, 175–221.

Tratnyek, P. G., & Johnson, R. L. (2006). Nanotechnologies for environmental cleanup. *Nano Today, 1*, 44–48.

Tratnyek, P. G., Scherer, M. M., Deng, B., & Hu, S. (2001). Effects of natural organic matter, anthropogenic surfactants, and model quinones on the reduction of contaminants by zero-valent iron. *Water Research, 35*, 4435–4443.

Usman, M., Hanna, K., & Haderlein, S. (2016). Fenton oxidation to remediate PAHs in contaminated soils: A critical review of major limitations and counter-strategies. *The Science of the Total Environment, 569–570*, 179–190.

Villa, R. D., Trovó, A. G., & Nogueira, R. F. P. (2010). Diesel degradation in soil by Fenton process. *Journal of the Brazilian Chemical Society, 21*, 1088–1095.

Vilve, M., Vilhunen, S., Vepsalainen, M., Kurniawan, T. A., Lehtonen, N., Isomaki, H., & Sillanpaa, M. (2010). Degradation of 1,2-dichloroethane from wash water of ion-exchange resin using Fenton's oxidation. *Environmental Science and Pollution Research International, 17*, 875–884.

Wang, C. B., & Zhang, W. X. (1997). Synthesizing nanoscale iron particles for rapid and complete dechlorination of TCE and PCBs. *Environmental Science & Technology, 31*, 2154–2156.

Wang, W., & Zhou, M. (2010). Degradation of trichloroethylene using solvent-responsive polymer coated Fe nanoparticles. *Colloids and Surfaces A, 369*, 232–239.

Wang, Q., Lee, S., & Choi, H. (2010). Aging study on the structure of Fe0-nanoparticles: Stabilization, characterization, and reactivity. *Journal of Physical Chemistry C, 114*, 2027–2033.

Wang, Y., Zhou, D., Wang, Y., Zhu, X., & Jin, S. (2011). Humic acid and metal ions accelerating the dechlorination of 4-chlorobiphenyl by nanoscale zero-valent iron. *Journal of Environmental Sciences, 23*, 1286–1292.

Wang, F., Wu, Y., Gao, Y., Li, H., & Chen, Z. (2016a). Effect of humic acid, oxalate and phosphate on Fenton-like oxidation of microcystin-LR by nanoscale zero-valent iron. *Separation and Purification Technology, 170*, 337–343.

Wang, L., Yang, J., Li, Y., Lv, J., & Zou, J. (2016b). Removal of chlorpheniramine in a nanoscale zero-valent iron induced heterogeneous Fenton system: Influencing factors and degradation intermediates. *Chemical Engineering Journal, 284*, 1058–1067.

Xu, L., & Wang, J. (2011). A heterogeneous Fenton-like system with nanoparticulate zero-valent iron for removal of 4-chloro-3-methyl phenol. *Journal of Hazardous Materials, 186*, 256–264.

Xu, X., Wo, J., Zhang, J., Wu, Y., & Liu, Y. (2009). Catalytic dechlorination of p-NCB in water by nanoscale Ni/Fe. *Desalination, 242*, 346–354.

Yan, W., Herzing, A. A., Li, X.-Q., Kiely, C. J., & Zhang, W. X. (2010). Structural evolution of Pd-doped nanoscale zero-valent Iron (nZVI) in aqueous media and implications for particle aging and reactivity. *Environmental Science & Technology, 44*, 4288–4294.

Yehia, F. Z., Eshaq, G., Rabie, A. M., Mady, A. H., & ElMetwally, A. E. (2015). Phenol degradation by advanced Fenton process in combination with ultrasonic irradiation. *Egyptian Journal of Petroleum, 24*, 13–18.

Yin, X., Liu, W., & Ni, J. (2014). Removal of coexisting Cr(VI) and 4-chlorophenol through reduction and Fenton reaction in a single system. *Chemical Engineering Journal, 248*, 89–97.

Yu, R. F., Chen, H. W., Cheng, W. P., Lin, Y. J., & Huang, C. L. (2014). Monitoring of ORP, pH and DO in heterogeneous Fenton oxidation using nZVI as a catalyst for the treatment of azo-dye textile wastewater. *Journal of the Taiwan Institute of Chemical Engineers, 45*, 947–954.

Yu, B., Jin, X., Kuang, Y., Megharaj, M., Naidu, R., & Chen, Z. (2015). An integrated biodegradation and nano-oxidation used for the remediation of naphthalene from aqueous solution. *Chemosphere, 141*, 205–211.

Zha, S., Cheng, Y., Gao, Y., Chen, Z., Megharaj, M., & Naidu, R. (2014). Nanoscale zero-valent iron as a catalyst for heterogeneous Fenton oxidation of amoxicillin. *Chemical Engineering Journal, 255*, 141–148.

Zhang, W. (2003). Nanoscale iron particles for environmental remediation: An overview. *Journal of Nanoparticle Research, 5*, 323–332.

Zhang, W.-X., Wang, C.-B., & Lien, H.-L. (1998). Treatment of chlorinated organic comtaminants with nanoscale bimetallic particles. *Catalysis Today, 40*, 387–395.

Zhang, X., Lin, Y.-M., Shan, X.-Q., & Chen, Z.-L. (2010). Degradation of 2,4,6-trinitrotoluene (TNT) from explosive wastewater using nanoscale zero-valent iron. *Chemical Engineering Journal, 158*, 566–570.

Zhang, R., Li, J., Shen, C. L. J., Sun, X., Han, W., & Wang, L. (2013). Reduction of nitrobenzene using nanoscale zero-valent iron confined in channels of ordered mesoporous silica. *Colloids and Surfaces A, 425*, 108–114.

Zhang, W., Gao, H., He, J., Yang, P., Wang, D., Ma, T., Xia, H., & Xu, X. (2017). Removal of norfloxacin using coupled synthesized nanoscale zero-valent iron (nZVI) with H2O2 system: Optimization of operating conditions and degradation pathway. *Separation and Purification Technology, 172*, 158–167.

Zheng, T., Zhan, J., He, J., Day, C., Lu, Y., McPherson, G. L., Piringer, G., & John, V. T. (2008). Reactivity characteristics of nanoscale zerovalent iron – silica composites for trichloroethylene remediation. *Environmental Science & Technology, 42*, 4494–4499.

Zhou, T., Li, Y., Ji, J., Wong, F.-S., & Lu, X. (2008). Oxidation of 4-chlorophenol in a heterogeneous zero valent iron/H2O2 Fenton-like system: Kinetic, pathway and effect factors. *Separation and Purification Technology, 62*, 551–558.

Zhou, H., Han, J., Baig, S. A., & Xu, X. (2011). Dechlorination of 2,4-dichlorophenoxyacetic acid by sodium carboxymethyl cellulose-stabilized Pd/Fe nanoparticles. *Journal of Hazardous Materials, 198*, 7–12.

Zhou, H., Shen, Y., Lv, P., Wang, J., & Li, P. (2015). Degradation pathway and kinetics of 1-alkyl-3-methylimidazolium bromides oxidation in an ultrasonic nanoscale zero-valent iron/hydrogen peroxide system. *Journal of Hazardous Materials, 284*, 241–252.

Zhu, B.-W., Lim, T.-T., & Feng, J. (2006). Reductive dechlorination of 1,2,4-trichlorobenzene with palladized nanoscale Fe0 particles supported on chitosan and silica. *Chemosphere, 65*, 1137–1145.

Zhu, B.-W., Lim, T.-T., & Feng, J. (2008). Influences of amphiphiles on dechlorination of a trichlorobenzene by nanoscale Pd/Fe: Adsorption, reaction kinetics, and interfacial interactions. *Environmental Science & Technology, 42*, 4513–4519.

Zhu, N., Luan, H., Yuan, S., Chen, J., Wu, X., & Wang, L. (2010). Effective dechlorination of HCB by nanoscale Cu/Fe particles. *Journal of Hazardous Materials, 176*, 1101–1105.